Parameterization of dust emission for the simulation of the yellow sand (Asian dust) event observed in March 2002 in Korea

Soon-Ung Park and Hee-Jin In

School of Earth and Environmental Sciences, Seoul National University, Seoul, Korea

Received 5 February 2003; revised 1 July 2003; accepted 18 July 2003; published 15 October 2003.

[1] An extraordinarily severe yellow sand event was observed in Korea for the period of 21–23 March 2002. This event has been simulated using the three-dimensional eulerian transport model with meteorological outputs of the Regional Data Assimilation and Prediction System (RDAPS) together with the statistically derived dust emission conditions from WMO 3 hourly synoptic reporting data for seven spring seasons (March–May) from 1996 to 2002 in East Asia. The statistically derived dust-rise conditions with the help of the Chinese soil map in the source regions are found to be the threshold wind speed of 9.5, 7.5, 6.0 and 9.2 m s^{-1} and the upper limit of relative humidity of 60, 35, 30% and 40% in the Gobi, Sand, Loess and Mixed soil regions, respectively. These dust-rise conditions are implemented to the eulerian long-range transport model to simulate the extraordinarily intensive yellow sand event observed in Korea in terms of temporal and spatial variations of dust concentrations, starting and ending times of the yellow sand event over the Korean peninsula. It is found that the model simulates quite well the observed concentrations of more than 1,000 $\mu g\ m^{-3}$ within the same order of magnitude and the starting and ending times of yellow sand in Korea within an hour. The spatial distribution of vertically integrated dust concentration in the model is quite well coincided with that of aerosol index obtained by total ozone mapping spectrometer (TOMS). The simulated dust particle sizes indicate that most of mass concentrations of dust in the source regions are mainly contributed by dust particles larger than PM_{10} whereas those at distant regions from the sources are largely attributed to the PM_{10} particles, suggesting the usefulness of the particle size spectrum in identifying the origin of a dust storm. The presently derived emission conditions enable to forecast the yellow sand event in Korea more reasonably than previously used conditions of threshold friction velocities. *INDEX TERMS:* 0305 Atmospheric Composition and Structure: Aerosols and particles (0345, 4801); 0345 Atmospheric Composition and Structure: Pollution—urban and regional (0305); 0368 Atmospheric Composition and Structure: Troposphere—constituent transport and chemistry; *KEYWORDS:* yellow sand, dust rise conditions, severe dust storm

Citation: Park, S.-U., and H.-J. In, Parameterization of dust emission for the simulation of the yellow sand (Asian dust) event observed in March 2002 in Korea, *J. Geophys. Res.*, *108*(D19), 4618, doi:10.1029/2003JD003484, 2003.

1. Introduction

[2] Yellow sand (Asian dust), which is a typical example of mineral aerosol frequently originates in the Sand desert, Gobi desert and Loess plateau in Northern China and Mongolia during the spring season [*In and Park*, 2002]. A severe dust storm was observed in Korea during 21–22 March in 2002. The maximum concentration of PM_{10} observed in the air pollution monitoring sites scattered over South Korea exceeded 1,000 $\mu g\ m^{-3}$ which is more than 10 times higher than that of the non-dust storm period. This severe dust storm has caused closing of most of airports and elementary schools in Korea.

[3] Recently the dust concentration of yellow sand observed in Korea has been increased with the gradual increase in arid regions in northeastern China due to desertification that might be caused by heavy cultivation, overgrazing and lack of precipitation in the source region [*Bai and Zhang*, 2001; *Park*, 2002].

[4] *In and Park* [2002] have simulated a very long lasted yellow sand event that was observed over Korea for the period of 14–24 April in 1998. This was reported to be transported to the western parts of USA across the Pacific Ocean. This case was simulated using a three-dimensional eulerian air quality model with the fifth-generation mesoscale model (MM5, Pennsylvania State University/National Center for Atmospheric Research) output of meteorological fields. They could simulate quite similar spatial distribution patterns of dust compared to that of aerosol index obtained by total ozone mapping spectrometer (TOMS; see http://toms.gsfc.nasa.gov). However, the simulated dust concentration was underestimated compared to the observed total suspended particulate (TSP) concentration in South Korea.

Copyright 2003 by the American Geophysical Union.
0148-0227/03/2003JD003484$09.00

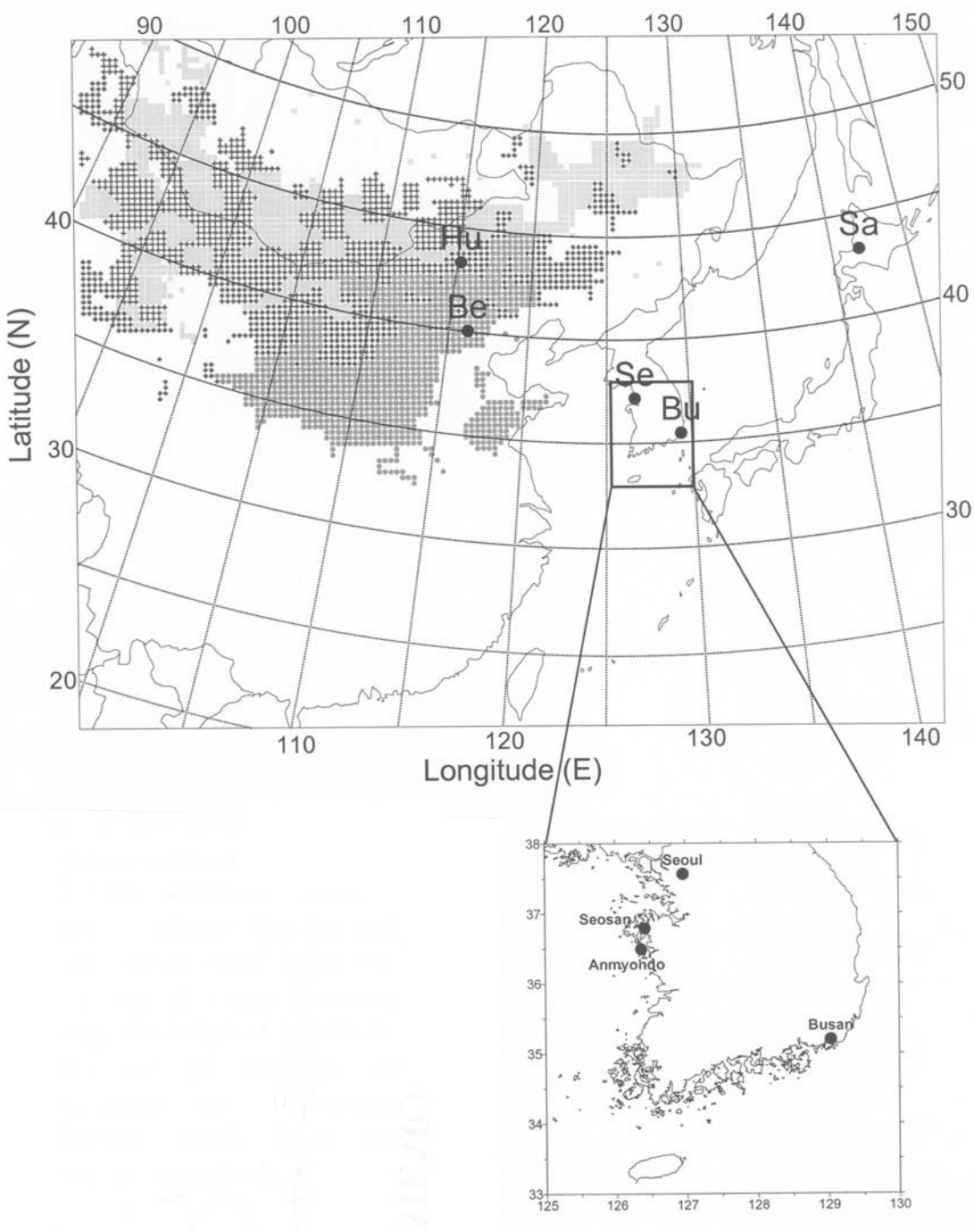

Figure 1. The model domain and yellow sand source regions (pluses, Gobi; diamonds, Sand; circles, Loess; rectangles, Mixed). The enhanced map shows South Korea with locations of several monitoring sites. The letters of Hu, Be, Se, Bu and Sa represent the locations of Hunsendake, Beijing, Seoul, Busan and Sapporo respectively.

This discrepancy might be caused by inaccurate delineation of source regions and emission amounts estimated by the threshold friction velocity that was based on the results of *Westphal et al.* [1987] and *Gillette* [1981].

[5] The purpose of this study is to improve the dust emission mechanism used in *In and Park* [2002] by using statistical analysis of the World Meteorological Organization (WMO) synoptic reporting data for seven years from 1996 to 2002 in the source regions and to simulate long-range transport of an intense yellow sand event observed during 21–22 March 2002 in Korea to understand important physical mechanisms of this event.

2. Model Description

2.1. The Meteorological Model

[6] The meteorological model used in this study is the operational meteorological model of the Regional Data

Assimilation and Prediction System (RDAPS) in Korea Meteorological Administration (KMA). This model is developed on the basis of MM5 version 3 and defined in the x, y, and σ coordinate with a horizontal resolution of 30 km and 33 vertical layers up to the 50 hPa level [*Grell et al.*, 1994; *Duhdia et al.*, 2001].

[7] The equation sets of RDAPS are non-hydrostatic primitive physical equations of momentum, thermodynamics and moisture with physical processes including the Kain-Fritsch scheme for convective parameterization, the mixed-phase scheme for moisture explicit scheme, the non-local boundary layer scheme for planetary boundary layer processes and the cloud-cooling scheme for radiation.

[8] The domain of the model is shown in Figure 1 with four source regions of yellow sand: the Sand, Loess, Gobi [*Chun*, 1996; *In and Park*, 2002] and Mixed soil using the Chinese soil map [*Yi*, 1986]. Mixed soil is a kind of mixed soil type that is difficult to be identified as Sand, Loess and/or Gobi. The simulation covers the first dust-rise report in the source region on 19 March to the end of the yellow sand event observed in Korea on 23 March 2002.

2.2. Aerosol Transport Model

[9] The aerosol model is exactly the same as in *In and Park* [2002] that includes physical processes such as three-dimensional advection, diffusion, dry and wet depositions in the σ coordinate system [*Westphal et al.*, 1987]. This aerosol model uses the meteorological output of RDAPS. The equatin is given by

$$\begin{aligned}\frac{\partial p_* C(r)}{\partial t} = &-\frac{\partial p_* C(r) u}{\partial x} - \frac{\partial p_* C(r) v}{\partial y} - \frac{\partial}{\partial \sigma} C(r)\left(p_* \dot{\sigma} + g\rho V_f\right) \\ &+ p_* \frac{\partial}{\partial x} K_h \rho \frac{\partial C(r)/\rho}{\partial x} + p_* \frac{\partial}{\partial y} K_h \rho \frac{\partial C(r)/\rho}{\partial y} \\ &+ \frac{g^2}{p_*} \frac{\partial}{\partial z} K_z \rho^3 \frac{\partial C(r)/\rho}{\partial z} + p_* C_0 + p_* S \end{aligned} \quad (1)$$

where $C(r)$ is the concentration of spherical particles of radius r, u and v the horizontal winds, V_f the fall velocity (positive downward), $p_* = p_{surf} - p_{top}$, p_{surf} the surface pressure, p_{top} the model top pressure, ρ the air density, g the gravitational acceleration, K_h the horizontal eddy diffusivity, K_z the vertical eddy diffusivity, C_0 the coagulation term and S the source and sink. In the model C_0 is neglected.

[10] The numerical method to solve equation (1) is described in detail by *In and Park* [2002] with proper initial and boundary conditions. The deposition processes of particles are included in the source and sink term in equation (1). Dry deposition uses the inferential method [*Wesely et al.*, 1985; *Wesely*, 1989] with taking into account the gravitational settling velocity computed by Stokes' law while wet deposition follows the Regional Acid Deposition Model (RADM) [*Dennis et al.*, 1993; *Walcek and Taylor*, 1986; *Chang et al.*, 1987, 1991].

[11] In calculating dust concentration, particles of 0.2–74 μm in diameter are divided into 11 size bins with the same logarithm intervals in Table 1.

[12] The dust concentrations of each size bin are given initially zero. A positive-definite zero-flux outflow boundary condition with an appropriate flow divergence restriction of the lateral boundary condition is used [*In and Park*, 2002].

Table 1. Particle Size Divisions

Bin Number	Range of Particle Diameter, μm	Mid Diameter, μm
1	0.20 ~ 0.50	0.35
2	0.50 ~ 0.82	0.66
3	0.82 ~ 1.35	1.09
4	1.35 ~ 2.23	1.79
5	2.23 ~ 3.67	2.95
6	3.67 ~ 6.06	4.87
7	6.06 ~ 10.00	8.03
8	10.00 ~ 16.50	13.25
9	16.50 ~ 27.25	21.88
10	27.25 ~ 45.00	36.13
11	45.00 ~ 74.00	59.50

2.3. Dust Emissions

2.3.1. Delineation of Dust-Emission Regions

[13] One of the largest uncertainties in the modeling for long-range transport of dust is the emission strength in source regions. Generally dust mobilization is known to initiate when the strong wind blows over the dry and sparse vegetation areas. Therefore the surface features play an important role in both the location of the source regions and the intensity of dust emissions [*Gillette*, 1979; *Gillette et al.*, 1982; *Nickling*, 1988, 1994; *Marticorena et al.*, 1997; *Marticorena and Bergametti*, 1995]. Until now many studies have been parameterized the uplifting process using the wind speed, soil water content and vegetation cover [*Tegen and Fung*, 1994]. The value of surface wind speed that dusts start to be raised is called the threshold wind speed and its corresponding friction velocity is called the threshold friction velocity [*Helgren and Prospero*, 1987; *Kalma et al.*, 1988; *Gillette et al.*, 1980, 1982; *Westphal et al.*, 1988].

[14] Most of studies on the threshold friction velocity and/or the threshold wind speed have been conducted on dust uplifts at the Sahara desert. Recently, *Gong et al.* [2003] have implemented a physically based dust emission scheme to East Asia for 2001 ACE-Asia. *Shao* [2001] has developed a dust emission model including saltation bombardment and aggregates disintegration mechanism. His model is physically sound, however, there are many difficulties involved in accurately determining the micro-physical quantities required for the estimation of dust emission. These difficulties can be alleviated by taking statistical analysis of physical parameters in the source regions based on routinely available reporting data.

[15] Some studies on the threshold friction velocity on dust storms in East Asia have been conducted based on synoptic surface observation data [*Chun*, 1996; *Chung*, 1996; *In and Park*, 2002]. *Chung* [1996] has used one value of the threshold friction velocity (60 cm s^{-1}) in the entire dust source regions in East Asia, while *Chun* [1996] has used three different values of the threshold friction velocity estimated under the neutral condition according to three distinctive surface soil types (Sand, Gobi and Loess soils) in the source regions: 67 cm s^{-1} for the Gobi, 50 cm s^{-1} for the Sand and 35 cm s^{-1} for the Loess. *In and Park* [2002] have taken into account the atmospheric stability in the estimation of the threshold friction velocity. They have estimated the threshold friction velocities of 60 cm s^{-1}, 50 cm s^{-1}, 40 cm s^{-1} in the Gobi, Sand, and Loess region, respectively

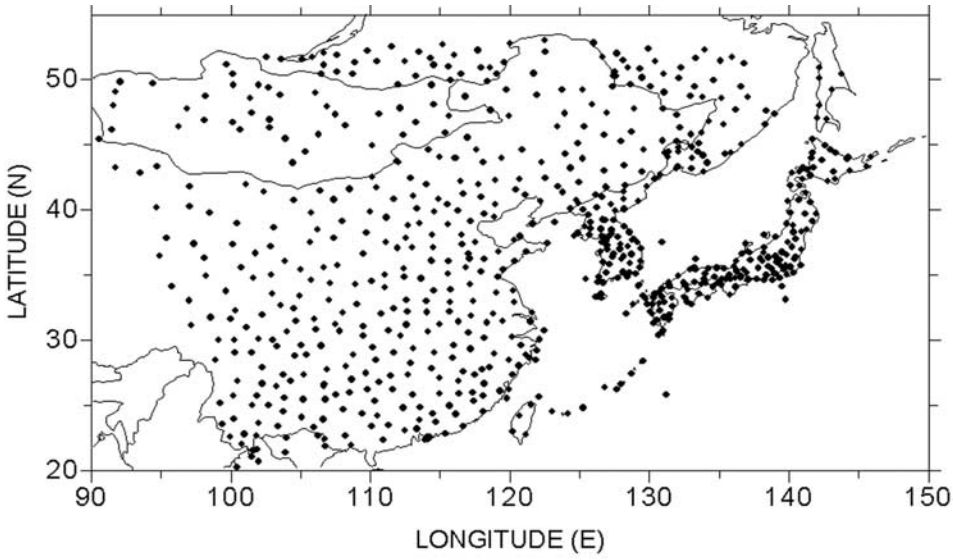

Figure 2. The geographical distribution of WMO surface reporting stations.

using the WMO synoptic reporting data. However, above mentioned studies had some limitations in delineating source regions of yellow sand due to insufficient reporting stations and short time series of data used. This study is some what extension of *In and Park* [2002] using more denser and longer time series of the WMO synoptic reporting data in the whole East Asian domain.

[16] Figure 2 shows locations of WMO synoptic stations in the analysis domain. More than 730 stations are located in the domain. Three hourly reporting present weather codes at these stations are analyzed to identify occurrence locations and frequencies of dust storms and dust rises for the period of seven springs (March–May) from 1996 to 2002 and the results are given in Figure 3. Dust storms and dust rises occur in the most of northern China and Mongolia with the maximum occurrence frequencies in the central southern parts of Mongolia, Badain Jaran and Tenggeri deserts in central northern China. Since the dust storms include not only the dust-rise but also the blowing dust, Figure 3 may not represent dust-emission source regions. To delineate the emission region of yellow sand, the soil type map in the analysis domain has been introduced. Figure 1 also shows the spatial distribution of four different types of soil (Gobi, Sand, Loess and Mixed soil) in the dust emission regions that are identified with the soil type map [*Yi*, 1986] and Figure 3.

2.3.2. Determination of Dust Emission Conditions

[17] The threshold wind speed is determined based on the 3 hourly observed wind speed, dust storm and dust rise reports, relative humidity, temperature, and precipitation at

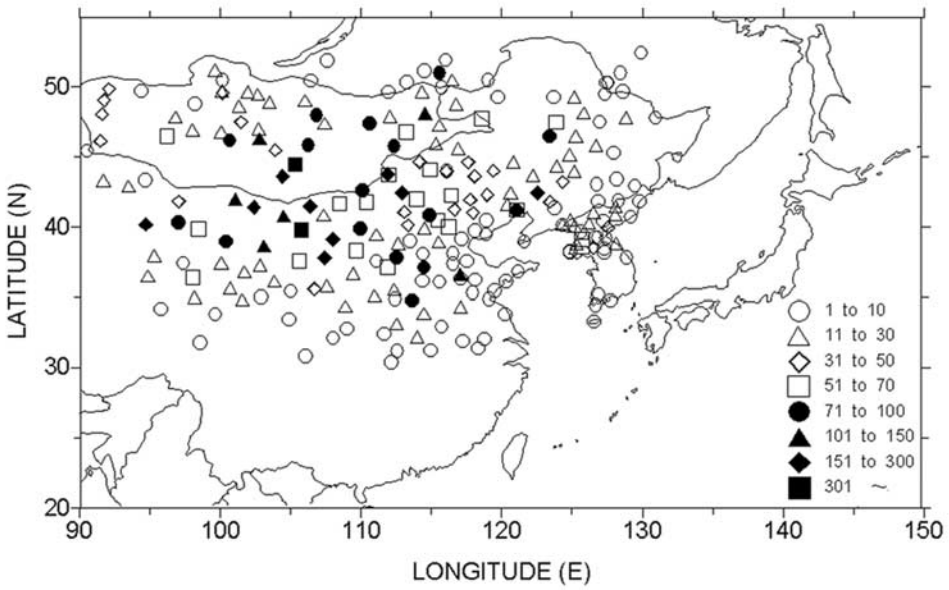

Figure 3. The spatial distributions of occurrence frequencies of dust storms and dust rises obtained from WMO 3 hourly surface reporting data for 7 springs (March to May) from 1996 to 2002.

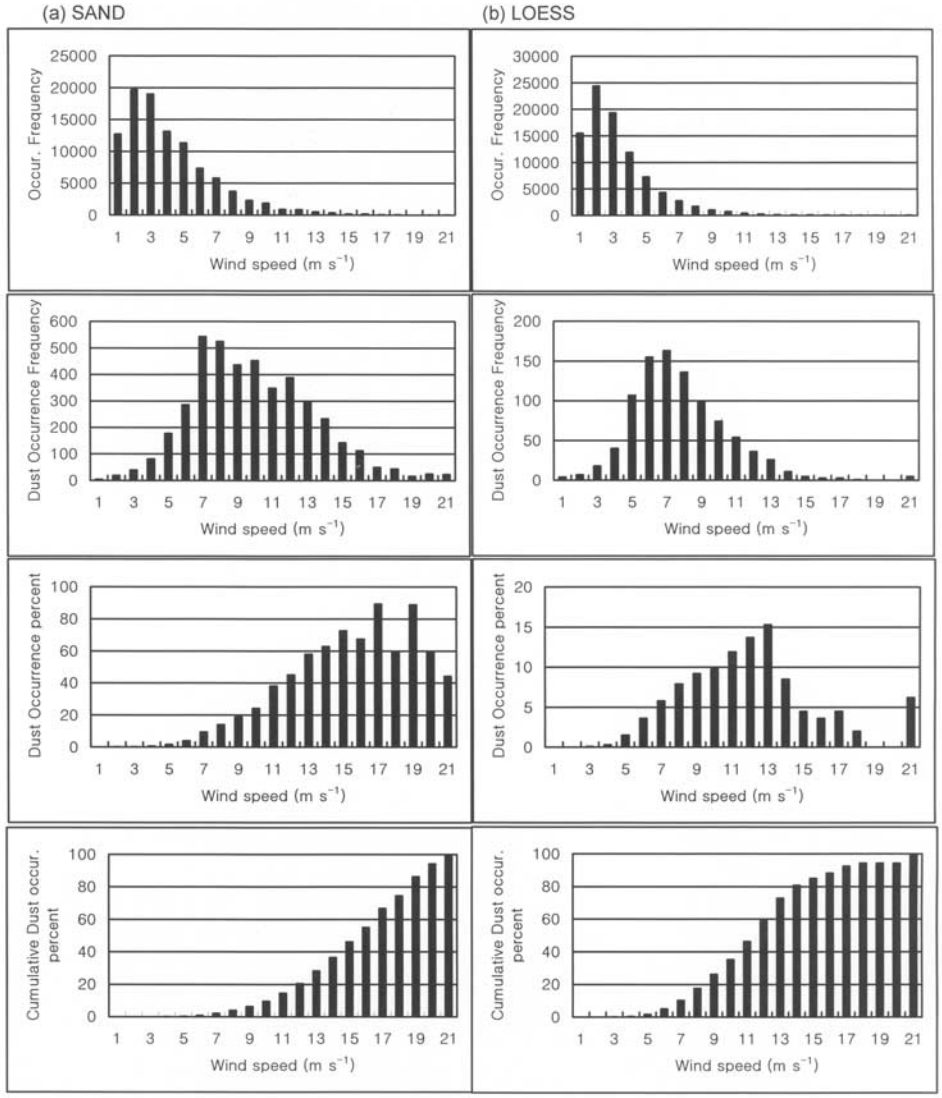

Figure 4. Occurrence frequencies of the wind speed, dust storm and/or dust rise, percent ratio of the occurrence frequency of dust rise to that of the wind speed and the normalized cumulative dust occurrence percentage with respect to the wind speed at the (a) Sand and (b) Loess region obtained from 3 hourly WMO surface reporting data for 7 spring seasons (March to May) from 1996 to 2002.

synoptic weather reporting stations (Figure 2) located in the source regions of the Gobi, Sand, Loess and Mixed soil (Figure 1). There are 162 WMO weather reporting stations in the source regions, among them 24 stations are in the Gobi region, 66 stations in the Sand region, 47 stations in the Loess region and 25 stations in the Mixed soil region. The data analysis indicates that there is no precipitation report at the station where dust storm or dust rise is reporting. This condition is used as one condition for the dust emission in the source regions. Figure 4 shows occurrence frequencies of wind speed, dust storm or dust-rise with respect to the wind speed, the ratio of the occurrence frequency of dust storm or dust-rise to that of the wind speed and the normalized cumulative ratio of the occurrence frequency of the dust storm or dust-rise to that of the wind speed with respect to the wind speed at various source regions. The threshold wind speed is defined as the wind speed at the normalized cumulative ratio of the dust occurrence frequency being 3.5%. This criteria yields the threshold wind speeds of 9.5, 7.5, 6.0, and 9.2 m s^{-1} at the Gobi, Sand, Loess and Mixed soil region, respectively (Figure 4).

[18] Figure 5 shows the occurrence frequency of relative humidity, the occurrence frequency of dust storm or dust-rise with respect to the relative humidity, the ratio of the occurrence frequency of dust storm or dust-rise to that of relative humidity and the normalized cumulative ratio of dust occurrence frequency at each source region. The distribution pattern of the ratio of dust occurrence frequency shows an exponential decrease with respect to increasing relative humidity at each source region. An exponential regression equation is applied to the dust occurrence ratio at each source region. The upper limit value of the relative humidity for the occurrence of the dust-rise is determined

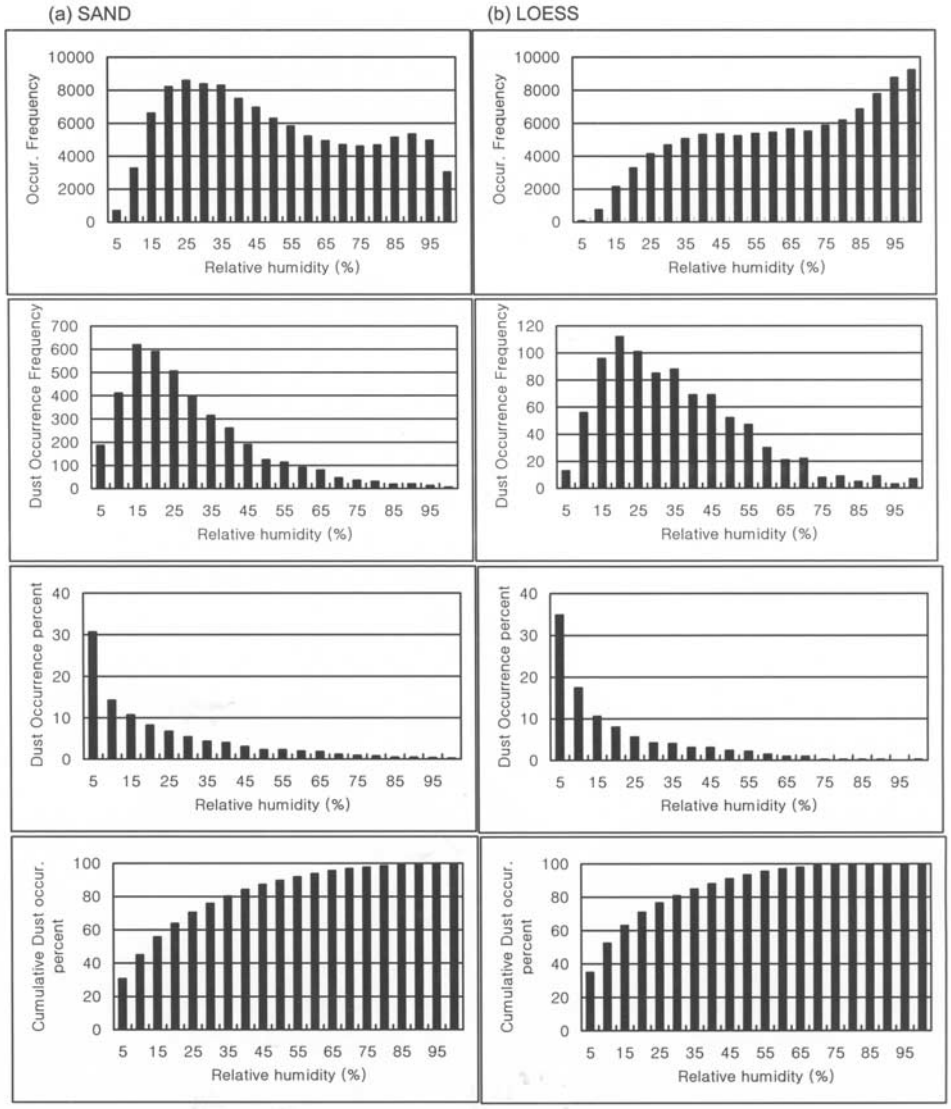

Figure 5. The same as in Figure 4 except for the relative humidity.

using the value of $e^{-1.5}$ of the optimum regression equation at each source region. This results in the upper limit value of the relative humidity of 60% for the Gobi, 35% for the Sand, 30% for the Loess and 45% for the Mixed soil (Figure 5). The correlation is calculated between the air temperature and the dust-rise frequency in the source region. However, the correlation is so poor that it is not taken into account as a dust-rise condition. Table 2 summarizes the conditions for the dust-rise in the source regions.

2.3.3. Estimation of Dust Emission Amounts

[19] *Westphal et al.* [1987] estimated source strength of dust particles of radii less that 10 μm as $F_a = 10^{-14}\ u_*^4$ based on the measurements of Saharan dust outbreaks [*Gillette*, 1981], where Fa is the dust flux from the surface and u_* is the friction velocity.

[20] The observed total suspended particle (TSP) concentration in Korea during the yellow sand event shows that the particles with the radius larger than 10 μm are rarely observed [*Meteorological Research Institute* (*METRI*)/*Korea Meteorological Administration* (*KMA*), 1998]. Thus particles with the radius larger than 37 μm are neglected at the present study. The total emission amounts of uplifted dust whose radius in the range of 0.1 ∼ 37 μm can be estimated as

$$\begin{aligned} F_a &= 7.117 \times 10^{-14} u_*^4 \quad \text{if } u_* \geq u_{*_t} \\ F_a &= 0 \qquad\qquad\qquad\quad \text{if } u_* < u_{*_t} \end{aligned} \tag{2}$$

where u_{*t} is the threshold friction velocity. The spectral mass distribution of the aerosol in the source region is

Table 2. Conditions for the Dust Rise in the Source Region

Source Region	Threshold Wind Speed, m s^{-1}	Upper Limit Relative Humidity, %	Precipitation
Gobi	9.5	60	none
Sand	7.5	35	none
Loess	6.0	30	none
Mixed soil	9.2	45	none

Table 3. U.S. Geological Survey Vegetation Categories with the Surface Roughness Length (Zo) and the Dust Emission Reduction Factor (R)

Type	Description	Zo, m	Reduction Factor (R)
A	Urban and built-up land	1.00	1.0
B	Dry cropland and pasture	0.02	0.4
C	Irrigated cropland and pasture	0.02	0.6
D	Mixed dry/irrigated cropland and pasture	0.02	0.5
E	Cropland/grassland	0.02	0.5
F	Cropland/woodland	0.02	0.7
G	Grassland	0.02	0.6
H	Shrubland	0.03	0.7
I	Mixed shrub/grassland	0.03	0.75
J	Savanna	0.02	0.8
K	Deciduous broadleaf forest	0.05	0.9
L	Deciduous needleleaf forest	0.05	0.9
M	Evergreen broadleaf forest	0.05	0.9
N	Evergreen needleleaf forest	0.05	0.9
O	Mixed forest	0.05	0.9
P	Water	0.001	1.0
Q	Herbaceous wet land	0.002	1.0
R	Wooded wet land	0.003	1.0
S	Barren or sparsely vegetated land	0.01	0.1
T	Herbaceous tundra	0.003	1.0
U	Wooded tundra	0.003	1.0
V	Mixed tundra	0.002	1.0
W	Bare ground tundra	0.001	1.0
X	Snow or ice	0.001	1.0

assumed to follow a power of 1.5 of the particle radius as by *Westphal et al.* [1987], in such a way that

$$\frac{dF_a}{d\ \log\ r} \propto r^{1.5} \tag{3}$$

where r is the radius of particle. The estimation of dust - emission flux using equation (2) requires the threshold friction velocity. This can be estimated by using the threshold wind speed in Table 2 with the information on the surface roughness length and atmospheric stability at each grid point in the source regions. The former is obtained from the land-use types and the letter from the meteorological model.

[21] Table 3 shows land - use types classified by the US geological survey vegetation categories in the source regions. 24 different types of the land-use and the corresponding surface roughness length are given in Table 3.

[22] The dust emission occurs in the arid desert and/or barren area with no vegetation. The vegetation covers in the source regions would reduce the dust emission flux. Thus reduction factors in Table 3 are applied to the dust emission in the source regions. The dust emission in a grid is given by

$$F_a = \sum_i (1 - f_i R_i) \times 7.117 \times 10^{-14} u_*^4 \qquad \text{if } u_* \geq u_{*_t} \tag{4}$$

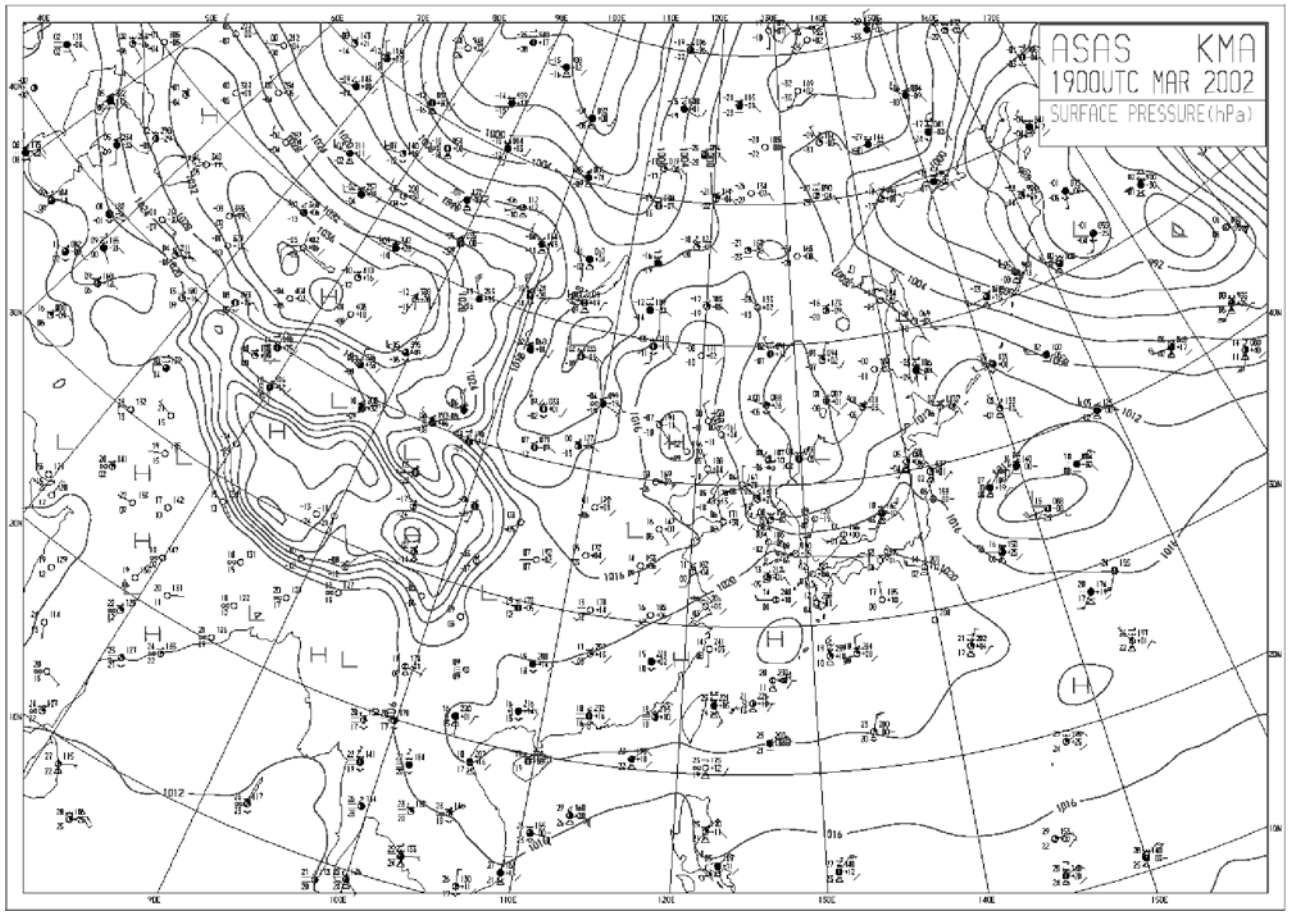

Figure 6. Surface weather charts on 0000 UTC (a) 19, (b) 20, (c) 21 and (d) 22 March 2002.

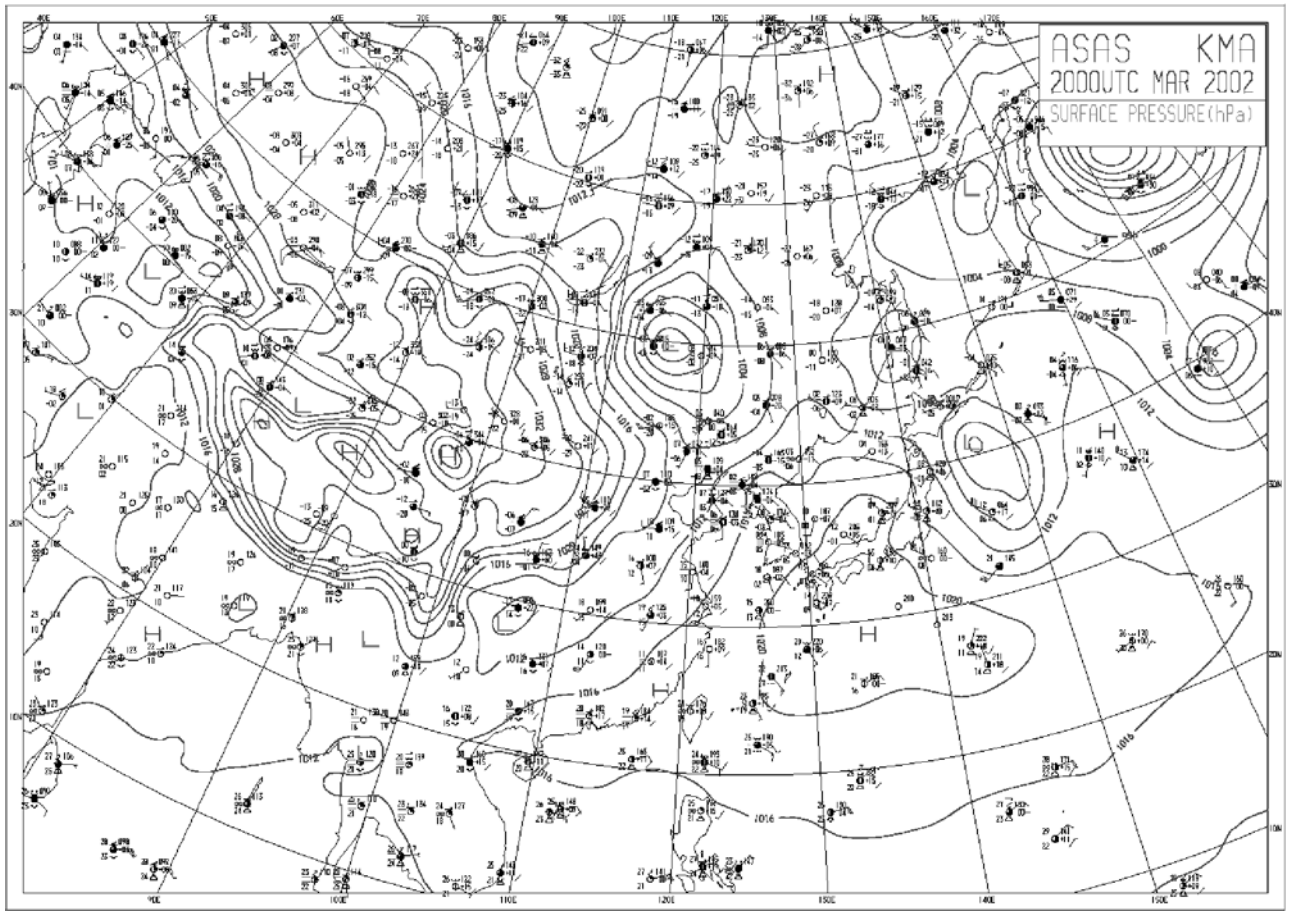

Figure 6. (continued)

where f_i is the fractional coverage of i type of vegetation and R_i is the reduction factor of i type of vegetation in a grid. The U.S. Geological Survey (USGS) satellite data with the horizontal resolution of 1 km are used for the determination of the vegetation coverage in each emission grid.

3. A Severe Yellow Sand Event Observed on 21–23 March 2002 in Korea

3.1. Synoptic Conditions of the Chosen Yellow Sand Event

[23] Figure 6 shows the 00 UTC surface weather charts on 19 to 22 March 2002. A surface low-pressure system was located at the south of Lake Baikal with a strong east-west surface pressure gradient to the west of the system at 00 UTC 19 March. Strong northerly winds exceeding 10 m s^{-1} prevailed in the west of the low-pressure system (Figure 6a). This low-pressure system gradually moved eastward with intensification to locate at 115 E and 50 N at 00 UTC 20 March (Figure 6b). The strong surface pressure gradient to the west of the low-pressure center provided a favorable condition for the dust-rise. In fact a lot of dust rises and blowing dusts were reported to the west of the low-pressure center (Figures 7b and c). As the low-pressure system kept to move eastward to locate at North East China at 00 UTC 21 March (Figure 6c) the raised dusts were transported southeastward over the northwestern parts of Korea and North East China (Figures 7d and e). At 00UTC 22 March (Figure 6d) the low-pressure system continued to move northeastward to locate at northeastern China with much relaxed surface pressure gradient to the west of it. At 12 UTC 21 March dust was raised newly over northern China (Figure 7f). This newly raised dust merged with the suspended dust was transported southeastward across the Korean peninsula to Japan until 23 March 2002 (Figures 7g–7j). This severe yellow sand event was completed after 12 UTC 23 March 2002 in northeast Asia.

3.2. Temporal Variations of the Dust Concentration Observed in Korea

[24] PM_{10} concentrations observed at two regular monitoring sites of Seoul and Busan in Korea (Figure 1) indicate that the dust storm moves southeastward across the Korean peninsula. At Seoul located to the northwestern part of Korea the PM_{10} concentration starts to increase rapidly from 0200 UTC 20 March to reach a maximum of more than 1,500 $\mu g\ m^{-3}$ at 1500 UTC 22 March. Thereafter a second dust storm is observed with a maximum concentration of 800 $\mu g\ m^{-3}$ at 0600 UTC 22 March 2002 (See Figure 15c). However, at Busan located at the southeastern tip of Korea PM_{10} concentrations begins to increase rapidly from 0700 UTC 21 to reach a maximum of more than 1000 $\mu g\ m^{-3}$ at some around 0800 UTC 21 March. Thereafter the high concentration level of more than

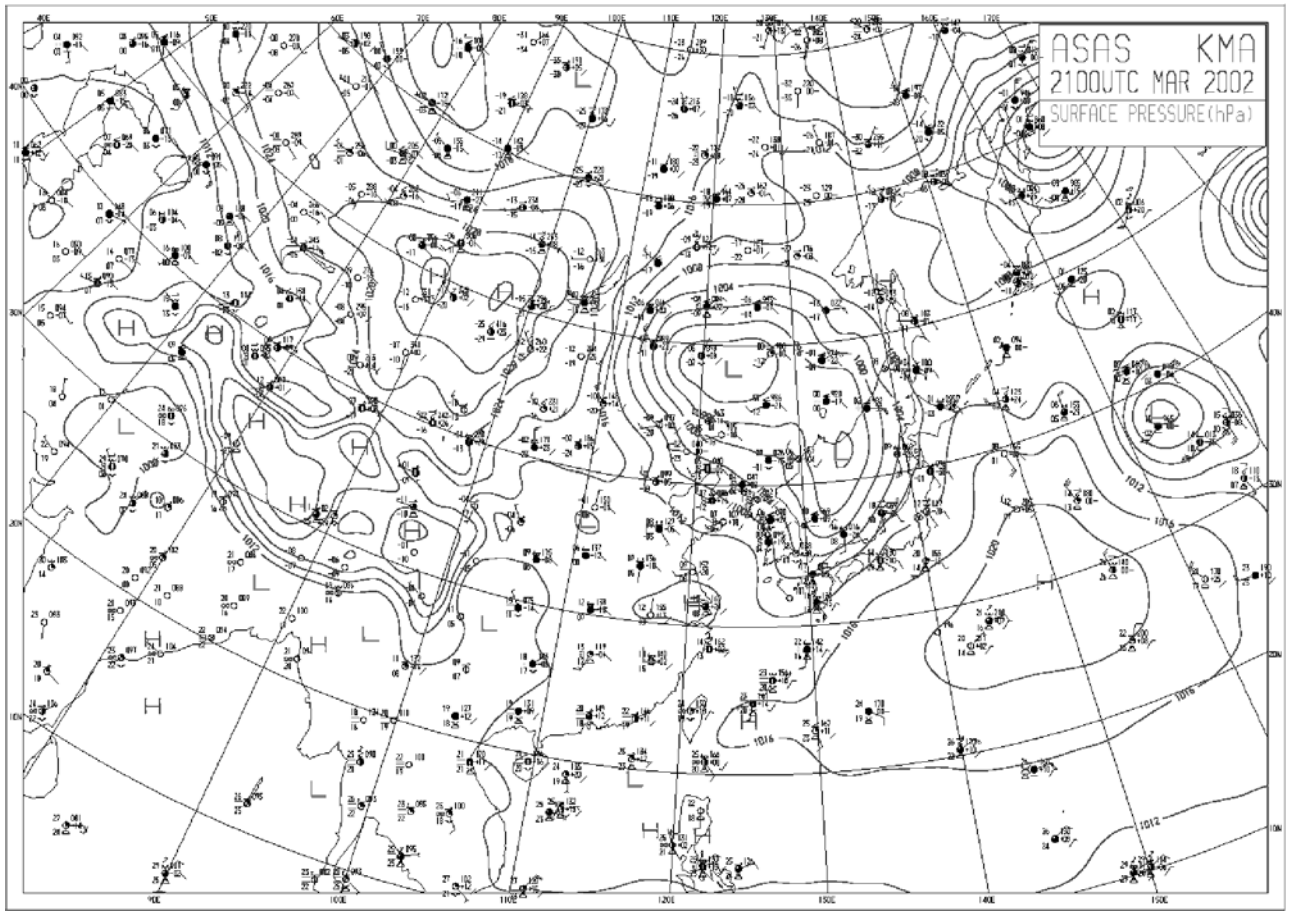

Figure 6. (continued)

1,000 μg m^{-3} keeps to remain until 0600 UTC 22 March when the first dust storm sweeps over the Korean peninsula. A second dust storm with a maximum PM_{10} concentration of 380 μg m^{-3} at 1500 UTC 22 passes over the Korean peninsula at 0800 UTC 22 March 2002 (See Figure 15d).

[25] Figure 8 shows the evolutionary feature of the aerosol extinction coefficient obtained from the Micro Pluse Lidar [*Spinhirne*, 1995] at Seoul during the yellow sand event period over South Korea. A strong extinction coefficient layer extends up to 700 m from the starting time of the measurement at 1200 LST to 1800 LST 21 March and then the extinction coefficient slightly decreases for about 1.5 hours in the lower layer. Thereafter a very high extinction coefficient occurs in the lower layer from 1930 LST 21 to 0500 LST 22 March. This feature is in good agreement with the observed PM_{10} concentration at the surface monitoring site of Seoul. The vertical extension of this high dust concentration layer reaches to 1.5 km above the ground at 2000 LST 21 and then gradually lowers to 500 m at around 500 LST 22 March. On the other hand, an upper level high dust layer at about 5.5 km above the ground appeared at around 1800 LST 21 March moves gradually downward to 1 km at 0700 LST 22 March with varying intensities. A second high extinction coefficient appears at 1 km above the ground at 1100 LST 22 and gradually moves downward to reach the ground level at around 1500 LST 22. Thereafter it becomes weakened until 1900 LST 22 March. At 2000 LST the dust layer extends up to 3 km with much intensification. The dust layer is rapidly weakened after 2200 LST 22 March 2002. There appears a dust layer at the 2 km height level at 900 LST 23 and lasts until 2000 LST 23 March without affecting the ground-level concentration (Figure 8).

[26] Figure 9 shows the averaged total number concentrations with respect to the particle size observed by the optical particle counter (OPC) before and during the dust storm over Korea at Anmyondo (Figure 1) which is a background monitoring site. Averaging has been done for one day of 20 March 2002 before the dust storm period whereas the 12-hour average has been done from 1200 LST to 2300 LST 21 March 2002 during the dust storm period. The calculated mass concentrations assuming a spherical shape of a particle with constant density of 2,600 kg m^{-3} are also given in Figure 9.

[27] During the dust storm period the number concentration of less than 0.5 μm particle decreases slightly whereas that of larger than 0.5 μm increases up to 10–100 times. The estimated maximum mass concentration before the dust storm is about 9 μg m^{-3} at the particle size of 2.23–3.67 μm whereas that during the dust storm period is about 500 μg m^{-3} at the particle size of 6.06–10.0 μm, suggesting not only large particle size but also high mass concentration in association with the dust storm.

[28] Figure 10 shows the temporal variation of the mass concentration converted from the hourly number concen-

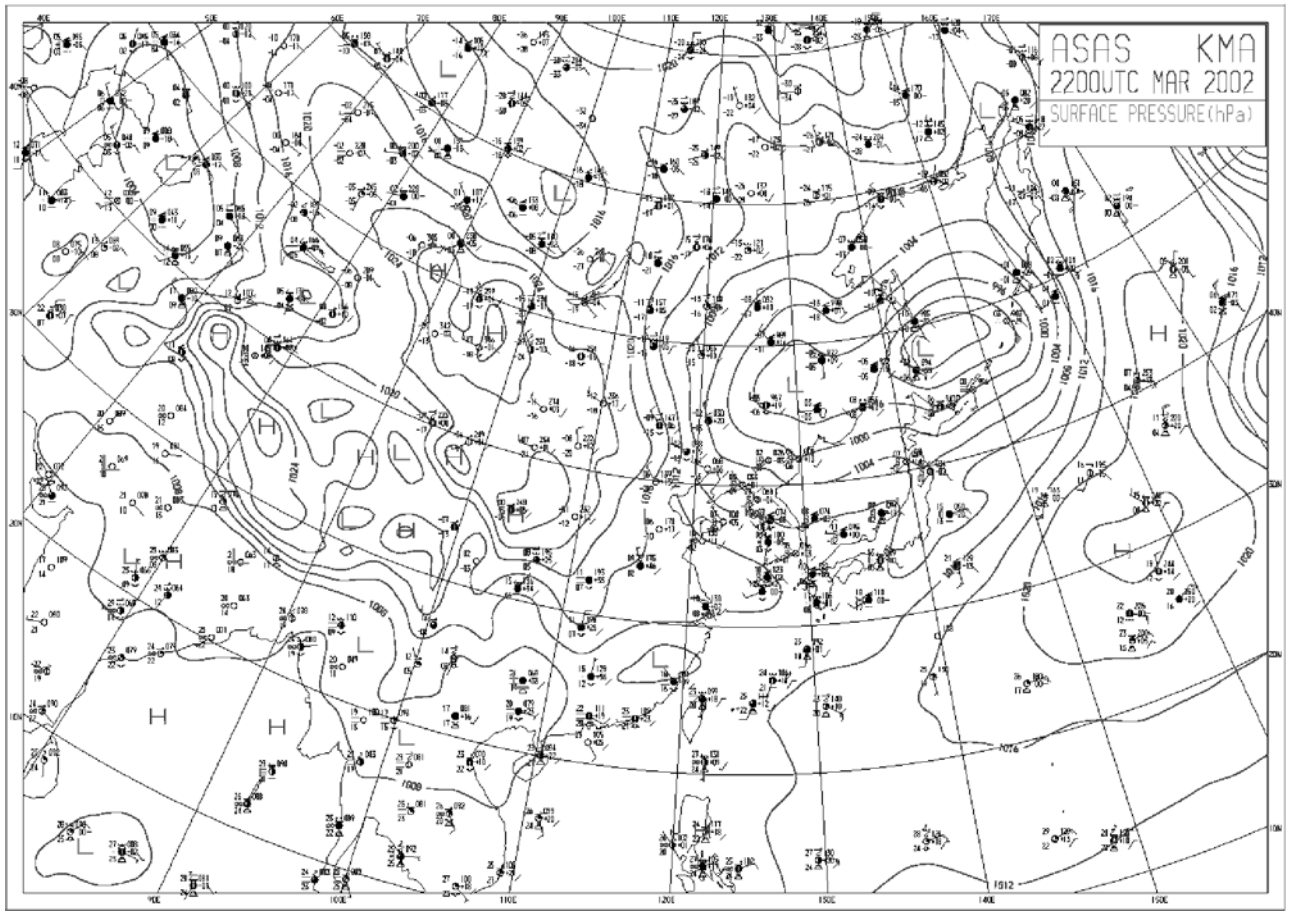

Figure 6. (continued)

tration measurement with respect to the particle size at Anmyondo for the period from 0100 LST 20 to 2400 LST 23 March 2002. We have calculated the mass concentrations of PM_{10} and PM_{25} assuming a spherical shape of the particle with the constant density of 2,600 kg m^{-3}. The converted PM_{10} mass concentration at the Anmyondo site is quite similar to the measured PM_{10} concentrations at Seosan that is the nearest air mornitoring site to Anmyondo (Figure 1). This implies that the density of the equivalent spherical shape of a dust particle seems to be 2,600 kg m^{-3}. The maximum PM_{10} concentration more than 1,000 μg m^{-3} occurs during 1500 LST to 2400 LST 21 March when the measured PM_{10} concentration at Seosan is missing.

3.3. Aerosol Index of Total Ozone Mapping Spectrometer (TOMS)

[29] Figure 11 shows the spatial distribution of aerosol index produced by Total Ozone Mapping Spectrometer (TOMS) during 20–23 March 2002. Relatively high value of aerosol index appeared in northeastern China on 20 March (Figure 11a) coincides with dust-rise and dust storm reports in Figure 7b. The dust rised in central northern China and the Loess region from 12 UTC 19 to 00 UTC 20 March (Figures 7b and c) moves southeastward to form an arc shape of aerosol band extending from central China to northeastward to the southern parts of North East China on 20 March (Figure 11a). This aerosol layer combined with new dust rise in northeastern China (Figure 7d) gradually moves southeastward to produce a very thick dust layer over the Korean Peninsula on 21 March (Figure 11b). As the low-pressure system moves northeastward the suspended dust layer behind this weather system also moves northeastward producing a dust layer zone extending northeast to southwest across the Korean Peninsula on 22 March (Figure 11c). Thereafter the dust layer progressively moves eastward to the East Sea and northern Japan on 23 March (Figure 11d). The high value of aerosol index in southern China (Figure 11) is not associated with yellow sand occurred in northeastern China. This is not included in this model.

4. Modeling Results

4.1. Dust Emissions

[30] Figure 12 shows the temporal variations of modeled dust emission area and its intensity in each source region. Significant diurnal variations of the emission area and the emission intensity occur in all source regions with the maximum emission area in the afternoon while the maximum emission intensity around noon time in associated with strong WMO reporting wind speeds in the afternoon in the source regions.

[31] The dust is raised in a large area of the Gobi source region (about 65% of the entire Gobi region of 6.4 $\times$

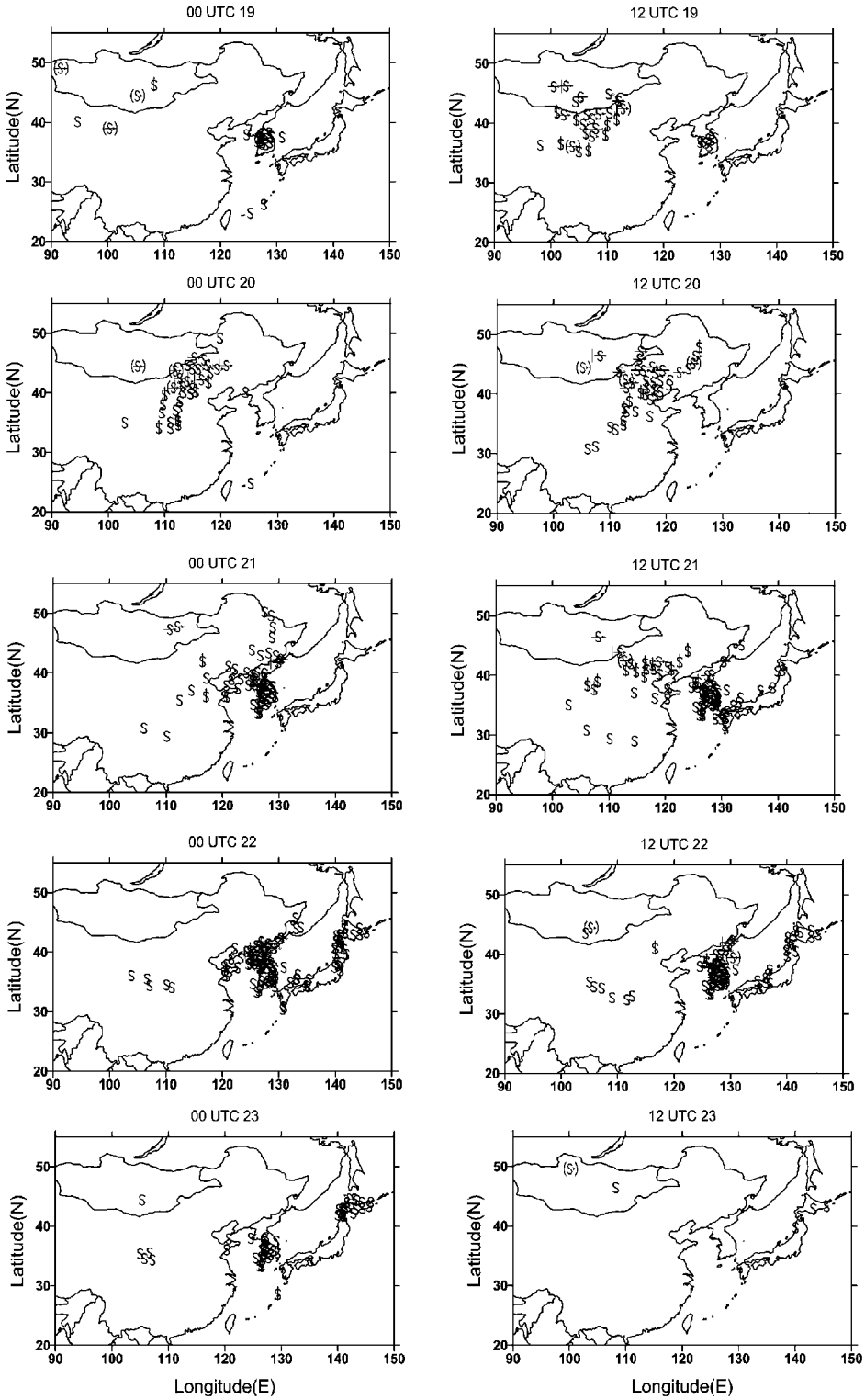

Figure 7. Spatial distributions of dust-rise denoted by S superposed by a vertical arrow, various intensities of dust storms denoted by S superposed by a single horizontal arraw and double horizontal arrow, and yellow sand (S) reporting sites from 19 to 23 March 2002.

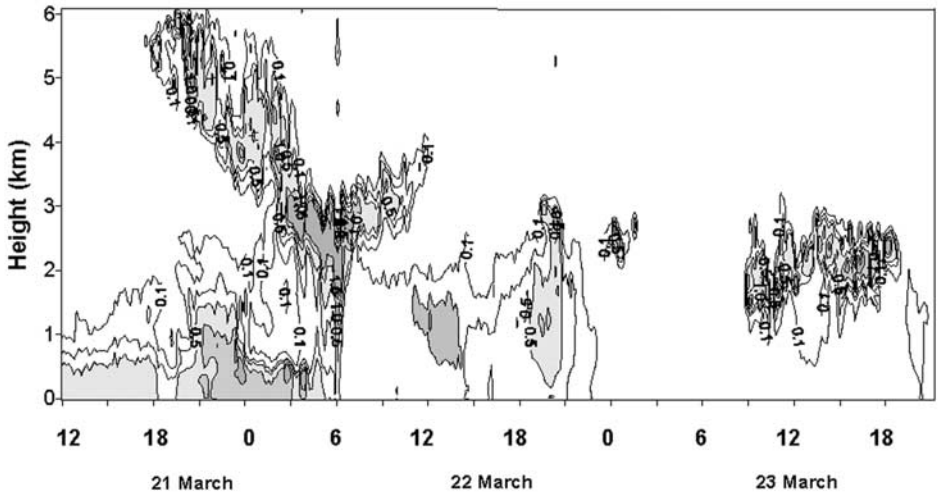

Figure 8. Aerosol extinction coefficient (km^{-1}) from Lidar observation at Seoul from 1200 LST 21 to 1800 LST 23 March 2002.

10^5 km^2) on 19 March, thereafter it gradually decreases until 21 March (Figure 12a). Likewise, the dust emission intensity reaches its maximum value on 19 March, thereafter it decreases gradually until 22 March with significant diurnal variations. Even though the emission area is small, the emission intensity is relatively large on 22 March in the Gobi region (Figure 12a), suggesting the time of occurrence of the maximum emission area being not coincided with that of emission intensity.

[32] In the Sand region (Figure 12b) the dust emission takes place throughout the entire analysis period from 19 to 23 March with significant day-to-day and diurnal variations. The maximum emission area occurs on 21 March (about 75% of the entire Sand area of 6.7×10^5 km^2), whereas the maximum emission intensity occurs on 19 March with the maximum value of 17 g m^{-2} h^{-1}. The mean emission intensity in the Sand region is about 4.4 g m^{-2} h^{-1} for the entire analysis period (Figure 12b). In the Loess region (Figure 12c), the dust is emitted throughout the entire analysis period with significant day-to-day and diurnal variations. A maximum emission area (about 65% of the entire Loess region of 8.4×10^5 km^2) occurs on 20 March while the maximum emission intensity (24 g m^{-2} h^{-1}) on 21 March. The mean emission intensity for the whole analysis period is about 4.5 g m^{-2} h^{-1} (Figure 12c) which is about the same as in the Sand region. In the Mixed soil region (Figure 12d) the evolutional pattern of the emission area and the emission intensity are quite similar to those in the Gobi region (Figure 12a). Both the maximum emission area (about 50% of the entire Mixed soil region of 8.5×10^5 km^2) and the maximum emission intensity (42 g m^{-2} h^{-1}) occur on 19 March. The average emission

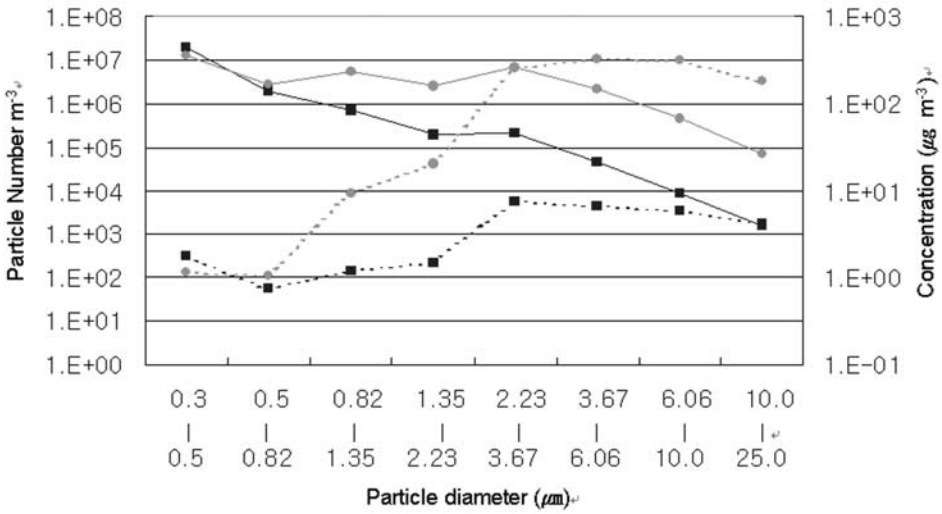

Figure 9. Observed total number concentrations (solid line, number of particle per m^3) and the converted mass concentrations (dotted line, μg m^{-3}) averaged before (denoted by squares; for one day of 20 March) and during (denoted by circles; from 1200 LST to 2300 LST 21 March) the dust storm over Korea at the Anmyondo site. See color version in HTML.

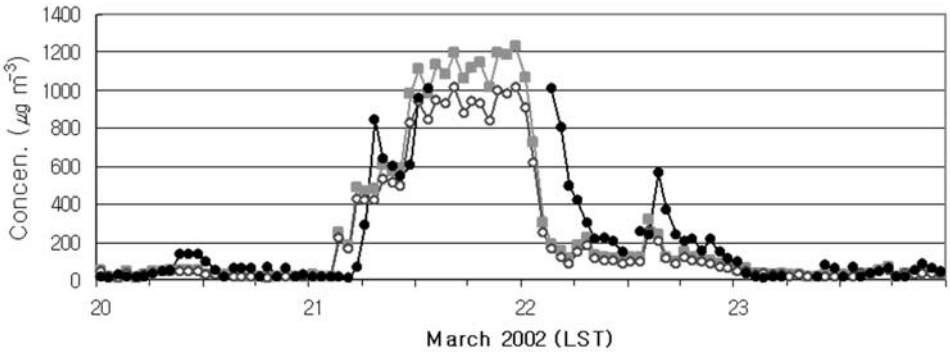

Figure 10. Temporal variations of the mass concentrations of PM_{10} (open circles) and PM_{25} (shaded squares) converted from the observed number concentrations with respective to the particle size at Anmyondo and the observed PM_{10} concentration (solid circles) at Seosan from 0100 LST 20 to 2400 LST 23 March 2002. See color version in HTML.

intensity for the whole analysis period is about 7.7 g m^{-2} h^{-1}, which is higher than those in the Sand and Loess regions but slightly lower than that in the Gobi region.

[33] The temporal variation of the averaged surface wind speed is quite similar to that of the dust emission in each source region (not shown here). The hourly maximum dust emission amount is about 13.6×10^6 t h^{-1} on 19 March in the Gobi region, 4.9×10^6 t h^{-1} on 21 March in the Sand region, 8.0×10^6 t h^{-1} on 21 March in the Loess region and 13.4×10^6 t h^{-1} on 19 March in the Mixed soil region. The total dust emission for the period from 19 to 23 March 2002 is 2.6×10^8 t, 1.4×10^7 t, 1.7×10^7 t, and 1.9×10^8 t in the Gobi, Sand, Loess, and Mixed soil regions, respectively.

4.2. Spatial Distributions of Dust

[34] The spatial distributions of the vertically integrated daily mean dust concentration with the wind vectors at the height of 1500 m ($\sigma = 0.82$) are shown in Figure 13. A large

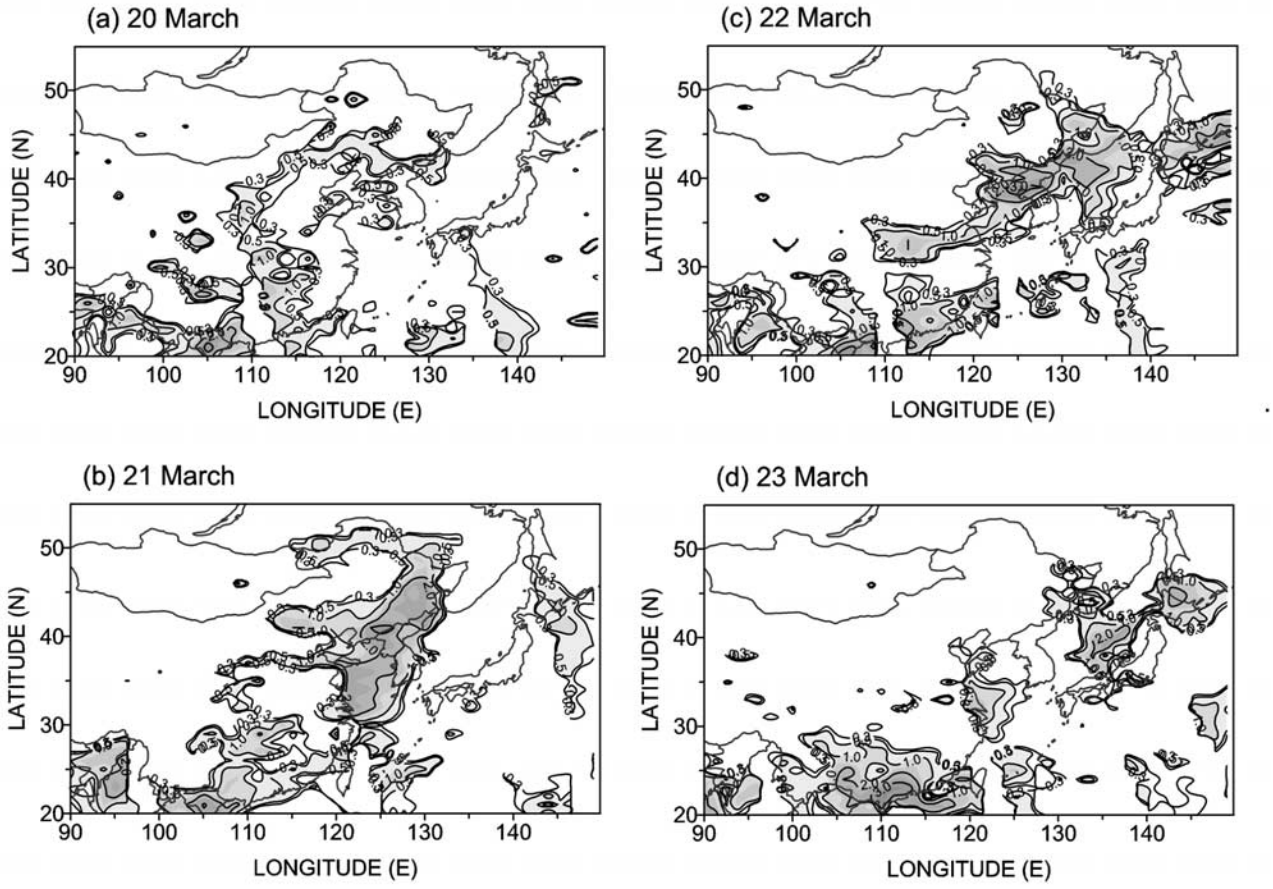

Figure 11. Spatial distributions of aerosol index obtained by TOMS on (a) 20, (b) 21, (c) 22 and (d) 23 March 2003. See color version in HTML.

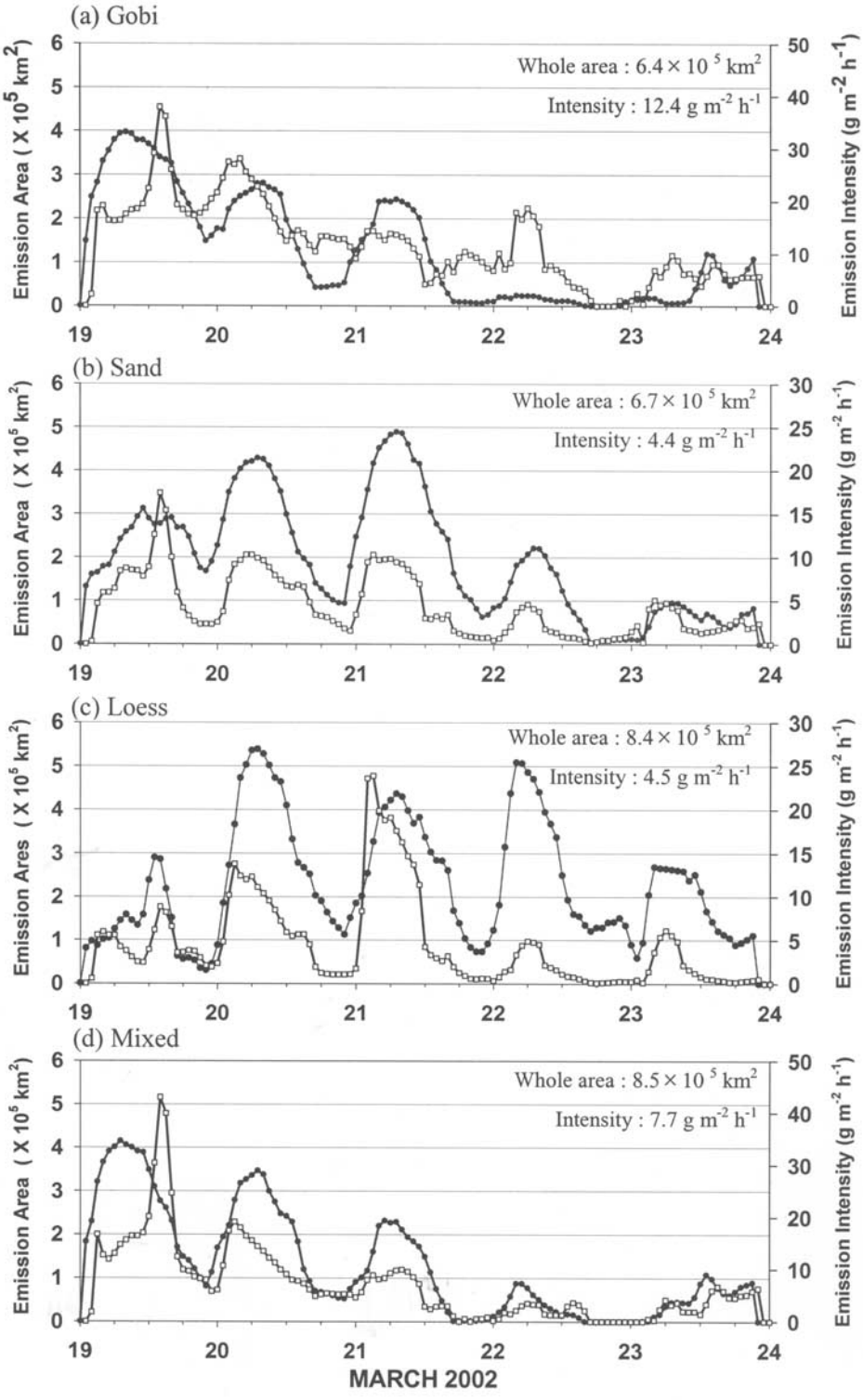

Figure 12. Time series of modeled dust emission area (solid circles, 10^5 km^2) and emission intensity (open squares, g m^{-2} h^{-1}) in the (a) Gobi, (b) Sand, (c) Loess and (d) Mixed soil regions.

amount of dusts emitted in southern Mongolia and central northern China on 19 March moves southeastward and continuously supplied by dusts emitted in northeastern China and the Loess region on 20 March yielding a wide area of dust laden air extending over North East China to central China. Thereafter, the dust laden air moves northeastward following the synoptic weather system (Figure 6), covering all over the Korean peninsula on 21 March. On 22 March, the northern parts of dust layer moves southeastward while the southern parts of dust layer moves east-northeast ward in association with wind fields. These dust-laden airs merge together over northern Japan.

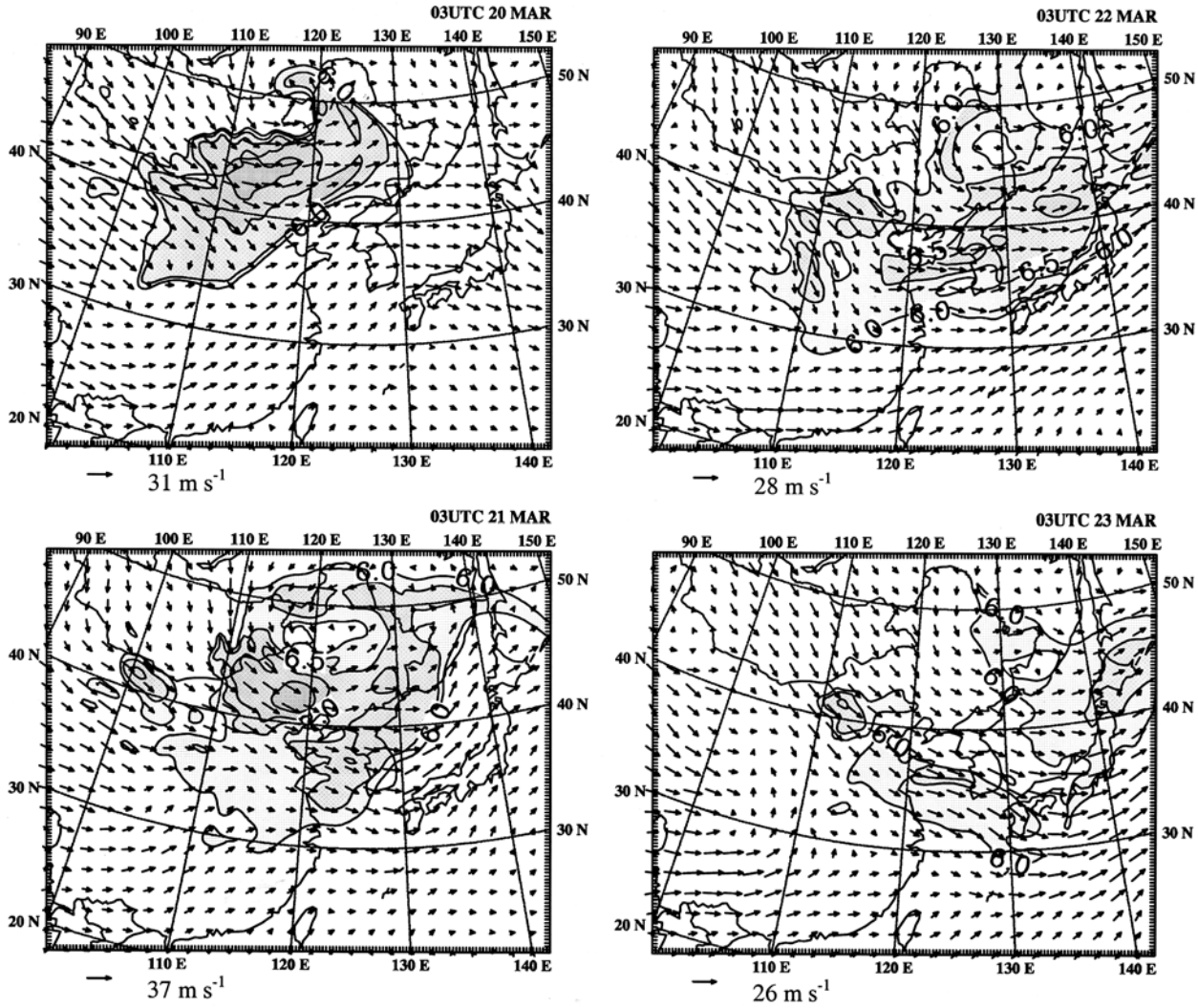

Figure 13. Spatial distribution of the vertically integrated TSP concentration expressed in common logarithm ($\mu g\ m^{-2}$) with the wind vector at the height of 1500m. The minimum contour is 6 with the interval of 0.5 in common logarithm. See color version in HTML.

[35] The time evolutionary pattern of the vertically integrated daily mean dust concentration (Figure 13) is quite resemble to that of the aerosol index obtained by TOMS (Figure 11).

4.3. Time-Height Cross Sections of the Dust Concentration at Seoul and Busan

[36] Figure 14 shows the time-height cross section of dust concentration with the potential temperature at Seoul and Busan in Figure 1. At both Seoul (Figure 14a) and Busan (Figure 14b) in Korea, the dust concentration increases in the upper layer first and then the maximum concentration layer moves progressively downward to reach the surface. The high concentration in the mixed layer occurred at Seoul and Busan on 21 and 22 March are caused by the dust storms occurred at the source site (Hunsendake) on 20 and 21 March, respectively. This can be identified by tracing the hourly simulated model concentration pattern. It is worthwhile to note that the time evolutionary feature of the vertical structure of the simulated dust concentration at Seoul (Figure 14a) is quite resemble to that of Lidar measurement in Figure 8, suggesting the usefulness of the present model in quantitative estimates of dust concentrations.

4.4. Temporal Variations of Dust Concentrations at Several Locations

[37] Figure 15 shows the time series of modeled PM_{10} concentrations averaged for the layers of below 100 m, 100–1,500 m and above 1,500 m above the ground at five sites shown in Figure 1. The estimated emission rates at the source site and Beijing while the observed PM_{10} concentrations at Seoul and Busan in Korea are shown in Figure 15. Among sites, the source site and Beijing belong to the source regions (Figures 15a and b) and are affected by dust emission directly. Therefore the PM_{10} concentration in the lowest level (below 100 m from the ground surface) tends to be maximum and decreases with height. However, away from source regions including Seoul (Figure 15c), Busan (Figure 15d) and Sapporo (Figure 15e), the maximum concentration tends to occur in the middle layer (100–

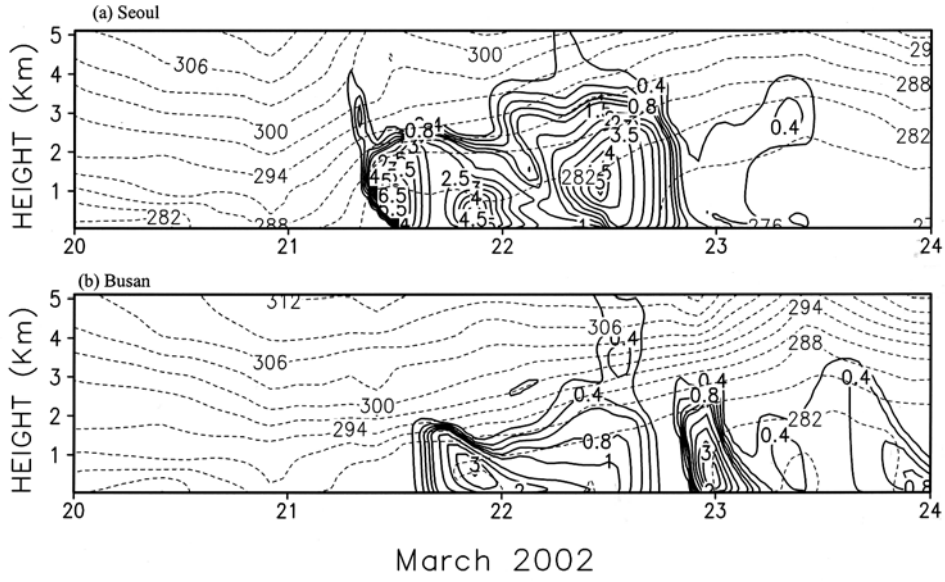

Figure 14. The time-height cross sections of dust concentration (solid line, 1000 μg m^{-3}) with the potential temperature (dashed line, K) at (a) Seoul and (b) Busan for the period of 00 LST 20 to 00 LST 24 March 2002.

1,500 m layer) first rather than in the lowest layer due to the effects of long-range transport and deposition. This could be seen more clearly in the time series of total dust concentration plots (not shown here) rather than PM_{10} concentration ones.

[38] The model simulates quite well the observed PM_{10} concentration at Seoul (Figure 15c). Two peak values of the observed PM_{10} concentration at Seoul are well simulated by the modeled PM_{10} concentration in the lowest layer with slightly different times of occurrences. However, the starting time of the yellow sand event observed in Korea coincides with that of concentration increase in the upper layer whereas the ending time of the event coincides with the time of the concentration in the lowest layer being near zero.

[39] The simulated maximum PM_{10} concentration at Busan (Figure 15d) is higher than 1,500 μg m^{-3}. However, the observed data are missing during the maximum occurring time due to the limitation of the maximum range (1,000 μg m^{-3}) of the measuring instrument. The model simulates quite well the time evolutionary feature and almost the same starting and ending times of the yellow sand event observed in Korea. This clearly suggests that the present model is able to predict the starting and ending time of a yellow sand event and its associated dust concentration quantitatively.

4.5. Particle Size Distributions

[40] The particle size is divided into three different classes for our convenience; Size 1 (the particle diameter, $D \leq 2.23$ μm), Size 2 (2.23 μm $D \leq 10$ μm) and Size 3 (10 μm $D \leq 74$ μm).

[41] The temporal variations of model estimated dust concentration at different height with different size spectra in the source region (Hunsendake) and away from the source region (Busan) are given in Figure 16. In the source region of Hunsendake (Figure 16a), the larger size (Size 3) has higher concentration in all layers with higher concentration reduction rate with height. The maximum mean concentration of larger particle (Size 3) of about 16,000 μg m^{-3} occurs at 1200 UTC 20 March in Layer 1 (below 100 m above the ground) whereas the PM_{10} concentration (sum of Size 1 and Size 2 concentrations) is about 2,700 μg m^{-3} at that time. This maximum concentration decreases with height to be about 15,000 μg m^{-3} in Layer 2 (100–1,500 m layer) and less than 1,000 μg m^{-3} in Layer 3 (above 1,500 m layer) for Size 3 with less or no reduction for PM_{10} concentration up to Layer 2. Above Layer 2 the concentration of PM_{10} is very low, suggesting high diffusive character of small particles in the boundary layer.

[42] It is worthwhile to note that the time series of the concentration of Size 3 has multipeak values in the lower layer (Layer 1). However, they become more simplified with height (Figure 16a). This is due to the fact that in the lower layer the concentration of Size 3 is controlled by both advection and local emission but the large particle (Size 3) has such a large terminal velocity that it cannot penetrates into higher level whereas the locally emitted large particles possibly penetrate into the upper layer resulting in high concentration in Layer 3 (Figure 16a). In fact, there are strong dust emissions at around 1000 UTC 20 and 0400 UTC 21 March at Hunsendake (Figure 15a) when the high concentrations of Size 3 occur in Layer 3 (Figure 16a).

[43] At Busan in Korea away from the source region (Figure 16b) the concentration of PM_{10} is much higher than that of Size 3 in all layers with a decreasing trend of concentration with height for the first dust storm observed from 0300 UTC to 0000 UTC 22 March at Busan. The maximum concentration of PM_{10} and Size 3 is about 1,800 μg m^{-3} and 600 μg m^{-3} in Layer 1, respectively but

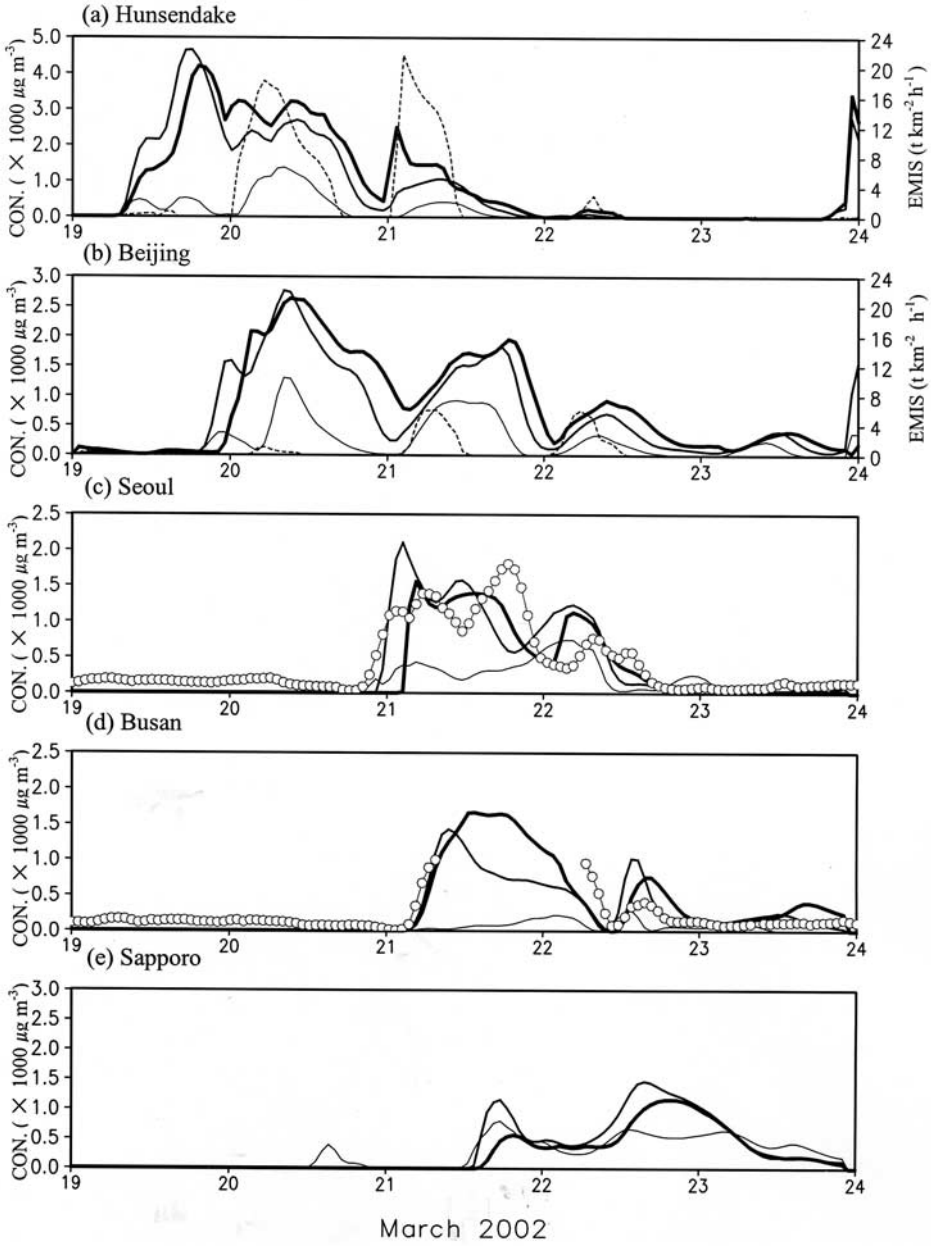

Figure 15. Time series of modeled mean PM_{10} concentration ($\times$ 1000 $\mu g\ m^{-3}$) averaged for the layers of surface to 100 m (thick solid line), 100–1500m (solid line), above 1500 m (thin solid line) with emission rates (dashed line , t $km^{-2}\ h^{-1}$) and observed surface PM_{10} concentrations (open circles) at (a) Husendake, (b) Beijing, (c) Seoul, (d) Busan and (e) Sapporo.

they become to about 1,500 $\mu g\ m^{-3}$ and 500 $\mu g\ m^{-3}$ in Layer 2 with much reduced concentrations in Layer 3 (Figure 16b). However, the second dust storm observed from 1000 UTC to 2100 UTC 22 March at Busan (Figure 16b) has different concentration distribution patterns with size. The concentration of Size 3 is much higher than that of PM_{10}. The maximum concentration of Size 3 is about 2,000 $\mu g\ m^{-3}$ but that of PM_{10} is about 700 $\mu g\ m^{-3}$ with a decreasing trend with height. The different distribution pattern of the concentration with size between the first dust storm and the second one observed at Busan suggests the different pathway of dust storms. The first dust storm observed in Korea seems to be originated further away from Korea than the second one.

4.6. Estimations of Dust Deposition

[44] Dry and wet deposition of dust have been estimated but the wet deposition of dust is not significant since the dust layer is always trailed by the precipitation system and the precipitation amount is small during the analysis. Therefore wet deposition is not shown here.

[45] Figure 17 shows the spatial distribution of daily total dry deposition of dust. A high dry deposition of dust zone whose dry deposition amount of more than

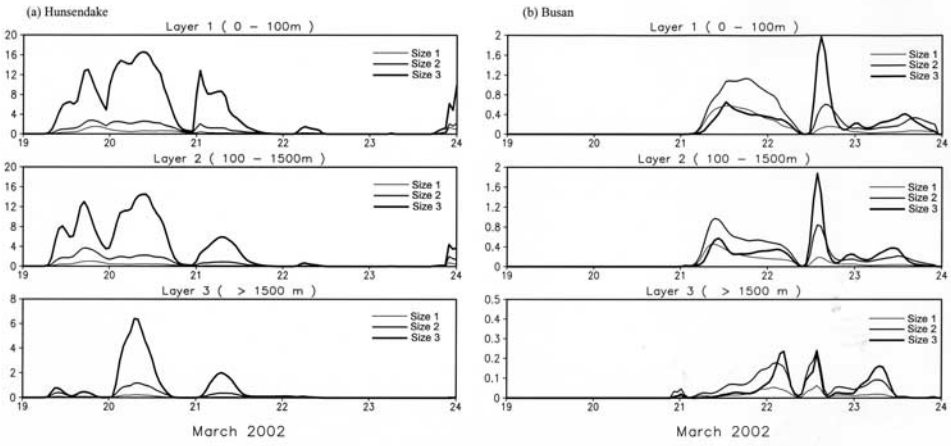

Figure 16. Temporal variations of modeled mean concentrations ($\times$ 1000 μg m^{-3}) of Size 1 (thin solid line, diameter $\leq$ 2.23 μm), Size 2 (solid line, 2.23 < diameter $\leq$ 10 μm) and Size 3 (thick solid line, diameter > 10 μm) at three different layers (Layer 1 $\leq$ 100 m, 100 < Layer 2 $\leq$ 1,500 m, and Layer 3 > 1,500 m) in the (a) source region (Hunsendake) and (b) away from the source region of Busan in Korea.

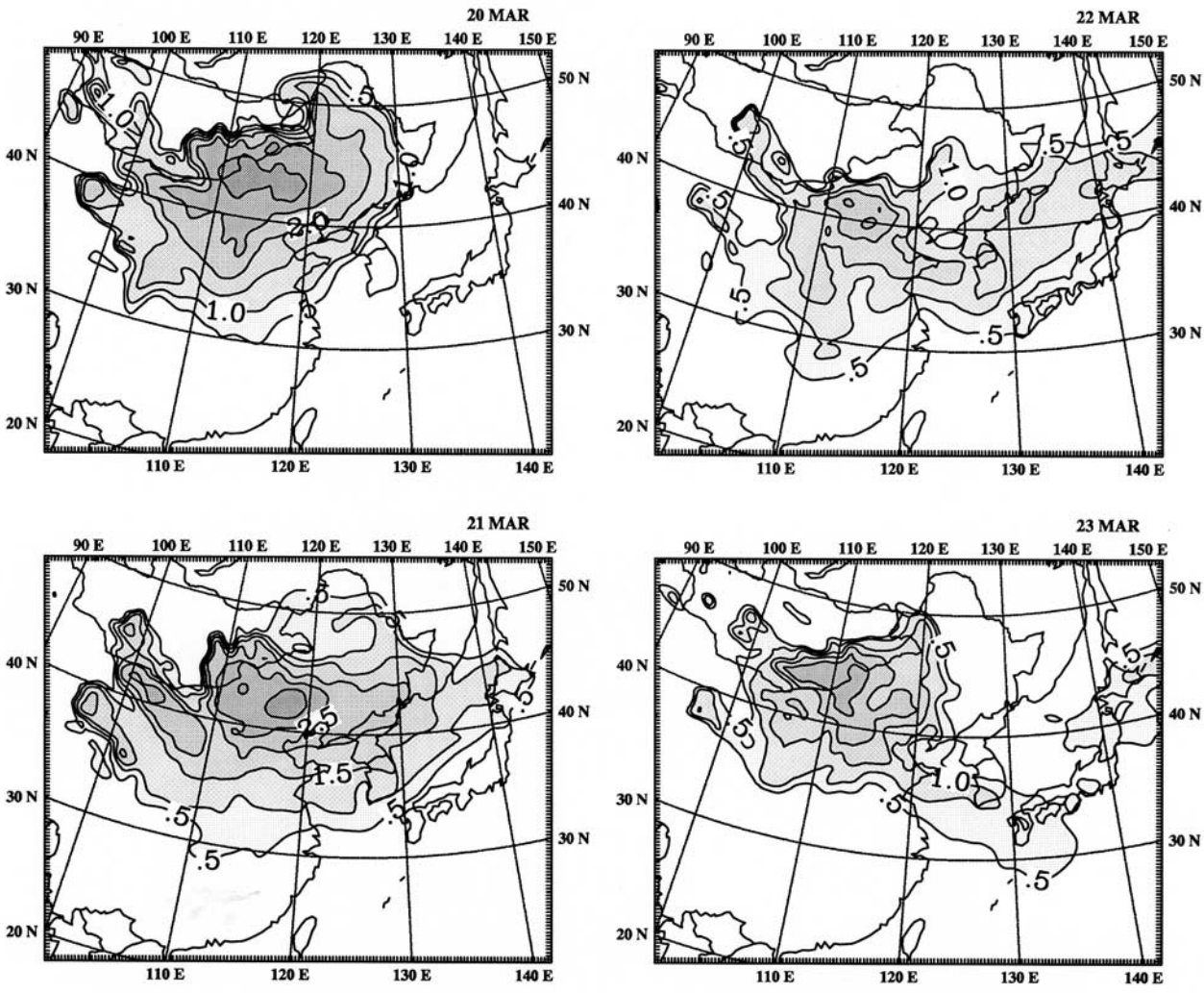

Figure 17. Spatial distributions of daily total dry deposition amount expressed in common logarithm (kg ha^{-1} day^{-1}) from 20–23 March 2002. See color version in HTML.

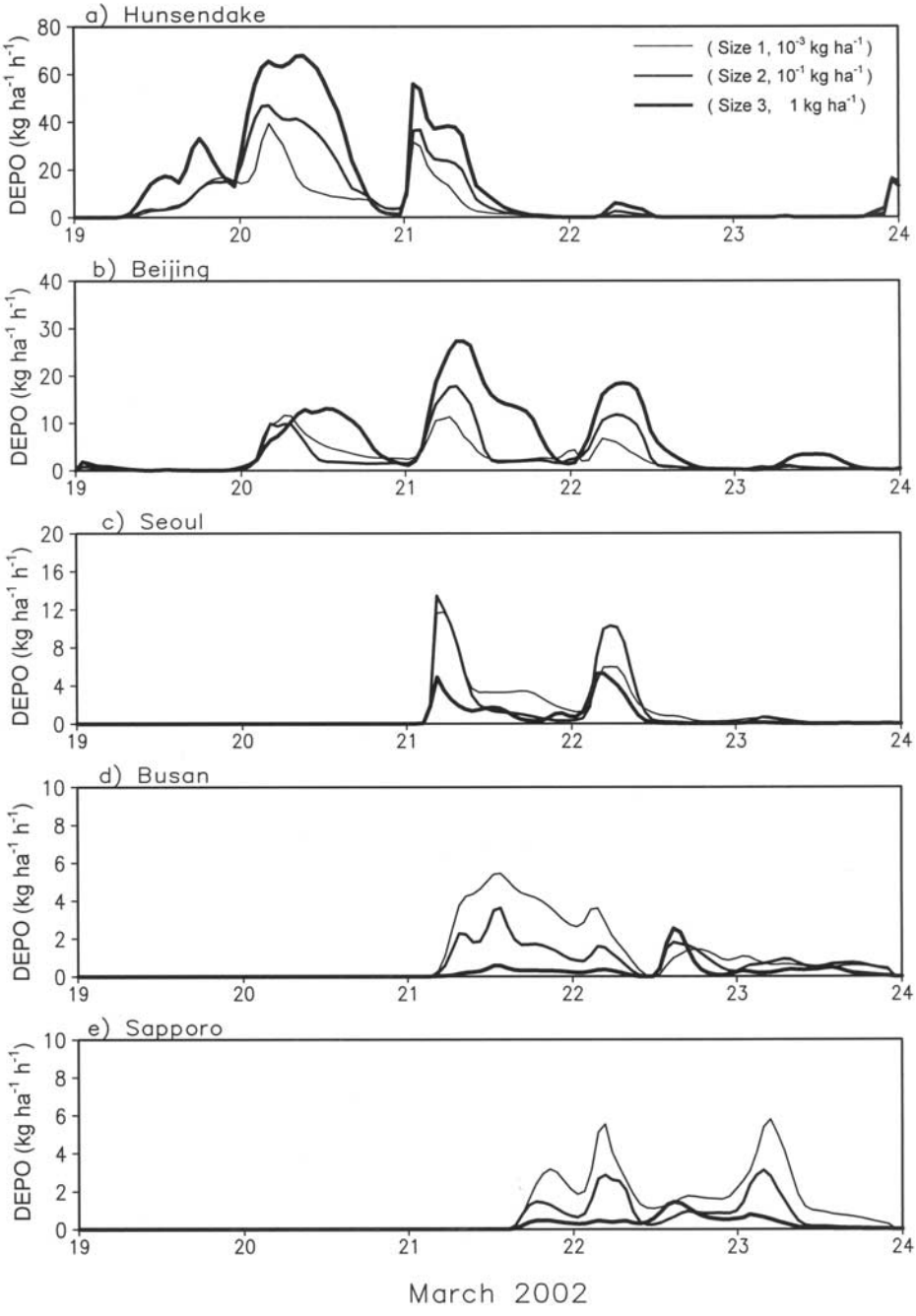

Figure 18. Temporal variations of dry deposition rate of Size 1 (thin solid line, 10^{-3} kg ha^{-1} h^{-1}), Size 2 (solid line, 10^{-1} kg ha^{-1} h^{-1}) and Size 3 (thick solid line, 1 kg ha^{-1} h^{-1}) at (a) Hunsendake, (b) Beijing, (c) Seoul, (d) Busan and (e) Sapporo.

1,000 kg ha^{-1} day^{-1} is located over northeastern China extending east-west direction parallel to 43°N latitude line on 20 March. This high dry deposition region is progressively extending to eastward to reach to the East Sea through the Korean peninsula on 21 March. Thereafter it turns to northeastward as the dust cloud moves northeastward following the weather system with much reduced deposition amount on 22 March. On 23 March the high deposition region is mainly confined in the source region of northeastern China.

[46] Figure 18 shows temporal variations of dry deposition of dust for different sizes at several sites shown in Figure 1. Most of dust deposition is contributed by large particles (Size 3) in all sites. However, the bigger the size the more the deposition rate, therefore dust deposition decreases with distance from the source region. The maximum deposition rate of Size 1, Size 2 and Size 3 in the source region (Figure 18a) on 20 March is 0.04 kg ha^{-1} h^{-1}, 4.5 kg ha^{-1} h^{-1} and 70 kg ha^{-1} h^{-1} respectively. However, at Beijing the maximum deposition rate is 0.01, 1.8 and

30 kg ha^{-1} h^{-1} for Size 1, Size 2 and Size 3 respectively on 21 March (Figure 18b). At Seoul that is located further away from the source region, the maximum dry deposition rate of dust is 0.012, 1.5 and 5 kg ha^{-1} h^{-1} for Size 1, Size 2 and Size 3 respectively on 21 March (Figure 18c). The dry deposition rate of large particles decreases remarkably with patch distance whereas that of smaller particles is of no significant. This tendency is more clearly seen at Busan (Figure 18d) and Sapporo (Figure 18e), where the dry deposition rate of Size 3 is rather smaller than that of Size 2. The maximum dry deposition rate of this event is 70 kg ha^{-1} h^{-1} on 20 March at Hunsendake, 30 kg ha^{-1} h^{-1} on 21 March at Beijing, 5 kg ha^{-1} h^{-1} on 21 March at Seoul, 2 kg ha^{-1} h^{-1} on 22 March at Busan and about 1 kg ha^{-1} h^{-1} on 22 March at Sapporo.

5. Summary and Conclusion

[47] A severe yellow sand event observed in Korea for the period of 21–23 March 2002 has been simulated using the three dimensional eulerian transport model with RDAPS meteorological outputs together with the statistically derived dust emission conditions using WMO 3 hourly synoptic reporting data for seven springs (March–May) from 1996 to 2002 in East Asia.

[48] The statistically analyzed WMO synoptic reporting data and the Chinese soil map are able to delineate the yellow sand (Asian dust) source regions and their soil types. The statistically derived dust-rise conditions in the source regions including the threshold wind speed and the upper limit of relative humidity are found to be 9.5, 7.5, 6.0 and 9.2 m s^{-1}, and 60, 35, 30 and 40% in the Gobi, Sand, Loess and Mixed soil regions, respectively. Precipitation is not reported at the dust-rise reporting sites. These dust-rise conditions are implemented to the eulerian long-range transport model to simulate extraordinarily intense yellow sand event observed in Korea.

[49] It is found that the evolutionary features of the spatial distribution of vertically integrated dust concentration in the model are quite well simulated the observed aerosol index obtained by TOMS. In addition, the model estimated PM_{10} concentration is simulated within the same order of magnitude and the starting and ending times of dust storms are also simulated almost the same time in Korea, suggesting the usefulness of the present model in forecasting the dust storm and the quantitative estimates of dust concentration.

[50] The simulated particles sizes suggest that the presently monitoring PM_{10} concentration in Korea may not represent the total dust concentration during the yellow sand event since the concentration of dust particles larger than PM_{10} are much higher than that of PM_{10}, especially when a dust storm occurs not far away from the Korean peninsula such as in the north of Beijing and the southern part of North East China in the desertification regions.

[51] The present study mainly pertains to long-range transport of dust without considering any chemical compositions and transformation with other pollutants during long-range transport that may be prerequisite for environmental impact assessment of yellow sand. This is now on hand.

[52] **Acknowledgments.** This research was supported by Korea Research Foundation Grant (KRF-2002-041-C00300). Special recognition goes to two anonymous reviewers for their helpful comments and to Eun-Hee Lee, a graduate student in Seoul National University for her skillful typing.

References

Bai, N., and K. Zhang, About sandstorms in China, 2000–2001, paper presented at 7th International Joint Seminar on the Regional Deposition Processes in the Atmosphere, Natl. Inst. for Environ. Stud., Tsukuba, Japan, 20–22 November 2001.

Chang, J. S., R. A. Brost, I. S. A. Isaksen, S. Madronich, P. Middleton, W. R. Stockwell, and C. J. Walcek, A three-dimensional Eulerian acid deposition model: Physical concepts and formulation, *J. Geophys. Res.*, *92*, 14,681–14,700, 1987.

Chang, J. S., et al., The regional acid deposition model and engineering model, *NAPAP Rep. 4*, Natl. Acid Precip. Assess. Prog., Washington, D. C., 1991.

Chun, Y.-S., Long range transport of yellow sand with special emphasis on the dust rise conditions in the source regions (in Korean), Ph.D. dissertation, 15 pp., Dept. of Atmos. Sci., Seoul Natl. Univ., Seoul, Korea, 1996.

Chung, K.-Y., Numerical simulations of yellow sand events observed in Korea, Ph.D. dissertation (in Korean), pp. 47–54, Dept. of Atmos. Sci., Seoul Natl. Univ., 1996.

Dennis, R. L., J. N. McHenry, W. R. Barchet, F. S. Binkowski, and D. W. Byun, Correcting RADM's sulfate underprediction: Discovery and correction of model errors and testing the corrections through comparisons against field data, *Atmos. Environ., Part A*, *27*, 975–997, 1993.

Duhdia, J., D. Gill, Y. R. Guo, K. Manning, J. Michalakes, W. Wang, and J. Wilson, PSU/NCAR Mesoscale modeling system tutorial class note and User's Guide: MM5 modeling system version 3, Natl. Cent. for Atmos. Res., Boulder, Colo., 2001.

Gillette, D. A., Environmental factors affecting dust emission by wind erosion, in *Saharan Dust*, edited by C. Morales, pp. 71–94, John Wiley, Hoboken, N. J., 1979.

Gillette, D. A., Production of dust that maybe carried great distances, *Spec. Pap. Geol. Soc. Am.*, *186*, 11–26, 1981.

Gillette, D. A., J. Adams, A. Endo, and D. Smith, Threshold velocities for input of soil particles in the air by desert soils, *J. Geophys. Res.*, *85*, 5621–5630, 1980.

Gillette, D. A., J. Adams, D. Muhs, and R. Kihl, Threshold velocities and rupture moduli for crusted desert soils for the input of soil particles into the air, *J. Geophys. Res.*, *87*, 9003–9015, 1982.

Gong, S. L., X. Y. Zhang, T. L. Zhao, I. G. Mckendry, D. A. Jaffe, and N. M. Lu, Characterization of soil dust distributions in China and its transporting during ACE-Asia 2: Model simulation and validation, *J. Geophys. Res.*, *108*(D9), 4262, doi:10.1029/2002JD002633, 2003.

Grell, G. A., J. Dudhia, and D. R. Stauffer, A description of the 5th generation Penn State/NCAR mesoscale model (MM5), *NCAR Tech. Note NCAR/TN-398*, 117 pp., Natl. Cent. for Atmos. Res., Boulder, Colo., 1994.

Helgren, D. A., and J. M. Prospero, Wind velocities associated with dust deflation events in the western Sahara, *J. Clim. Appl. Meteorol.*, *26*, 1147–1151, 1987.

In, H.-J., and S.-U. Park, A simulation of long-range transport of yellow sand observed in April 1998 in Korea, *Atmos. Environ.*, *36*, 4173–4187, 2002.

Kalma, J. D., J. G. Speight, and R. J. Ludwig, Potential wind erosion in Australia: A continental perspective, *J. Clim.*, *8*, 411–428, 1988.

Marticorena, B., and G. Bergametti, Modeling the atmospheric dust cycle: 1. Design of a soil-derived dust emission scheme, *J. Geophys. Res.*, *100*, 16,415–16,430, 1995.

Marticorena, B., G. Bergametti, B. Aumont, Y. Callot, C. N'Doumé, and M. Legrand, Modeling the atmospheric dust cycle, 2. Simulation of Saharan dust sources, *J. Geophys. Res.*, *102*, 4387–4404, 1997.

Meteorological Research Institute (METRI)/Korea Meteorological Administration (KMA), Intensive observation and analysis of aerosol in spring in Seoul, 1998.

Nickling, W. G., The initiation of particle movement by wind, *Sedimentology*, *31*, 111–117, 1988.

Nickling, W. G., Aelioan sediment transport and deposition, in *Sediment Transport and Depositional Processes*, edited by K. Pye, pp. 293–350, Blackwell Sci., Boston, Mass., 1994.

Park, S.-U., Field survey of yellow sand source regions, paper presented at Workshop of Asian Dust, Korean Meteorol. Admin., Korea, 22 March 2002.

Shao, Y., A model for mineral dust emission, *J. Geophys. Res.*, *106*, 20,239–20,254, 2001.

Spinhirne, J. D., Compact eye safe lidar systems, *Rev. Laser Eng.*, *23*, 112–118, 1995.

Tegen, I., and I. Fung, Modeling of mineral dust in the atmosphere: Sources, transport, and optical thickness, *J. Geophys. Res.*, *99*, 22,897–22,914, 1994.

Walcek, C. J., and G. R. Taylor, A theoretical method for computing vertical distributions of acidity and sulfate production within cumulus clouds, *J. Atmos. Sci.*, *43*, 339–355, 1986.

Wesely, M. L., Parameterization of surface resistance to gaseous dry deposition in regional-scale numerical models, *Atmos. Environ.*, *23*, 1293–1304, 1989.

Wesely, M. L., D. R. Cook, R. L. Hart, and R. E. Speer, Measurements and parameterization of particulate sulfur dry deposition over grass, *J. Geophys. Res.*, *90*, 2131–2143, 1985.

Westphal, D. L., O. B. Toon, and T. N. Carlson, A two-dimensional Investigation of the dynamics and microphysics of Saharan dust storms, *J. Geophys. Res.*, *92*, 3027–3049, 1987.

Westphal, D. L., O. B. Toon, and T. N. Carlson, A case study of mobilization and transport of Saharan dust, *J. Atmos. Sci.*, *45*, 2145–2175, 1988.

Yi, H., The soil atlas of China, in *Academia Sinica*, pp. 1–12, Cartogr. Publ., Beijing, China, 1986.

H.-J. In and S.-U. Park, School of Earth and Environmental Sciences, Seoul National University, Seoul 151-742, Korea. (supark@snupbl.snu.ac.kr)